TÉCNICO LISBOA

Vibration Energy Harvesting for LPWAN Connected Devices

Hugo Miguel Maltez Cunha

Thesis to obtain the Master of Science Degree in

Electronics Engineering

Supervisor: Prof. Luís Filipe Soldado Granadeiro Rosado

Examination Committee

Chairperson: Prof. Paulo Ferreira Godinho Flores

Supervisor: Prof. Luís Filipe Soldado Granadeiro Rosado

Member of the Committee: Prof. Artur Fernando Delgado Lopes Ribeiro

November 2021

Declaration

I declare that this document is an original work of my authorship and that it fulfils all the requirements of the Code of Conduct and Good Practices of the Universidade de Lisboa.

Declaração

Declaro que o presente documento é um trabalho original da minha autoria e que cumpre todos os requisitos do Código de Conduta e Boas Práticas da Universidade de Lisboa

Abstract

Vibration energy harvesting has been, in recent years, the recurring object of a variety of research efforts aimed toward providing an autonomous solution to the power supply of small-scale electronic devices. Energy harvesting is the process in which energy is captured from a system's environment and converted into usable electric power. Vibration sources provide energy that can be harvested to charge wireless sensors or produce electricity.

This thesis presents a brief explanation of the theory behind the phenomenon of harvesting and some of the transducers used for this purpose. It clarifies how energy is obtained from vibration using transducers with three different physical principles, through a piezoelectric material, a variation in capacitance (electrostatic), and a magnet and a coil (electromagnetic).

The magnetic levitation vibration energy harvesting transducer is the basis of this thesis; its structure and characteristics are presented in the beginning of this document. A transducer based on magnetic levitation is also elaborated, and the procedure used in its construction is explained. A characterization setup was developed to allow the analysis of the operation and behaviour of the transducer, when applied to different vibration sources. The instrumentation used in the characterization setup is presented and, thanks to that instrumentation, it is possible to analyse the transducer when a sinusoidal wave is applied to the vibration generator and when an arbitrary wave that originates a simulation of real sources is applied.

Keywords: Energy Harvesting, Vibration Energy, Electromagnetic Transducer, Magnetic Levitation Transducer, Transducer Characterization.

Resumo

Nos últimos anos o armazenamento de energia através da vibração tem sido objeto recorrente de estudos e pesquisas com o intuito de encontrar uma solução autónoma para alimentar dispositivos eletrónicos de pequena escala. O armazenamento de energia é o processo pelo qual a energia que deriva de fontes externas, é capturada e armazenada. As fontes de vibração fornecem energia que pode ser usada para alimentar sensores sem fios ou produzir eletricidade.

Esta tese apresenta uma breve explicação sobre a teoria dos três principais métodos mais populares e amplamente estudados. Esclarece também como a energia é obtida através da vibração nos três tipos de transdutores mais importantes, através de um material piezoelétrico, através de uma variação na capacidade de um condensador (eletrostática) e através de um íman e uma bobina (eletromagnética).

O transdutor de captura de energia da vibração por levitação magnética é a base da tese, é inicialmente apresentada a sua estrutura e características. É também elaborado um transdutor com base na levitação magnética e explicado o procedimento que foi feito na sua construção. Foi desenvolvido um *setup* de caracterização para permitir a análise do funcionamento e do comportamento do transdutor, quando aplicado a diferentes fontes de vibração. A instrumentação presente no *setup* de caracterização é apresentada e graças a essa instrumentação é possível analisar o transdutor, tanto quando uma onda sinusoidal é aplicada ao gerador de vibração como quando é aplicada uma onda arbitrária que origina uma simulação de fontes de vibração reais.

Palavras-Chave: Captura Energética, Energia da Vibração, Transdutor Eletromagnético, Transdutor por Levitação Magnética, Caracterização do Transdutor

Content

Chapter 1 Introduction 1

1.1 Purpose and motivation 1

1.2 Objectives 1

1.3 Document's Organization 2

Chapter 2 State of the Art 3

2.1 Energy Harvesting 3

2.2 Piezoelectric Transduction 4

2.2.1 Piezoelectric Harvester Design 5

2.3 Electrostatic Transduction 6

2.3.1 Electret free 6

2.3.2 Electret based 8

2.4 Electromagnetic Transduction 10

2.4.1 One-Magnet Spring-Based Electromagnetic Energy Harvester 11

2.4.2 Flux-guided Magnet Stacks Electromagnetic Energy Harvester 11

2.4.3 Magnetic Levitation Vibration Energy Harvesting Transducer 12

2.5 Commercial Solutions 13

2.5.1 HIPER-D 13

2.5.2 ModelC 14

2.5.3 ModelD 14

Chapter 3 Characterization setup 16

3.1 Architecture 16

3.2 Vibration Generator and Transducer Coupling Mechanism 17

3.3 Signal Generator 19

3.4 Data acquisition 20

3.5 Processing and control software 21

3.5.1 Transducer Characterization 22

3.5.2 Evaluation of Emulated Vibration Sources 23

Chapter 4 Transducer Design 28

Chapter 5 Results 32
5.1 Transducer Characterization Results 32
5.2 Evaluation of Emulated Vibration Sources Results 41
Chapter 6 Conclusion 46
6.1 Summary and Achievements 46
6.2 Future work 47
References 48

List of Figures

Figure 1- Piezoelectric transducer schematic. 4
Figure 2- Coupling modes for piezoelectric transductors: (a) '33' mode; and (b) '31' mode. 5
Figure 3- Basic cantilever beam energy harvester structure. 5
Figure 4- Cantilever beam energy harvester structure using permanent magnets. 6
Figure 5- Charge-constrained cycle. 7
Figure 6- Charge-constrained cycle graph. 7
Figure 7- Voltage-constrained cycle. 8
Figure 8- Voltage-constrained cycle graph 8
Figure 9 - Charge circulation of electret-based electrostatic conversion. 9
Figure 10- Model of an electromagnetic vibration transducer [12]. 10
Figure 11- One-Magnet Spring-Based Electromagnetic Energy Harvester design [13]. 11
Figure 12- Flux-guided Magnet Stacks Electromagnetic Energy Harvester design [14]. 12
Figure 13- Maglev Electromagnetic Energy Harvester design [16] 13
Figure 14- Hiper-D transducer and its characteristics. 14
Figure 15- ModelC transducer. 14
Figure 16- ModelD transducer. 15
Figure 17- Characterization setup interaction with the transducer. 16
Figure 18- Characterization setup. 17
Figure 19- Vibration generator 2185.00 17
Figure 20- Printed parts connections 18
Figure 21- Base part connections 18
Figure 22- Intermediate part connections. 19
Figure 23- Screw installation. 19
Figure 24- ADXL337 accelerometer. 20
Figure 25- Programmable Resistance Substituter 21
Figure 26- USB-6009 DAQ. 21
Figure 27- Transducer characterization front panel 22
Figure 28- Model characterization front panel. 23
Figure 29- Vibration sources chosen to simulate. 24
Figure 30- Vibration source to simulate front panel. 25
Figure 31- Input signal programming front panel 26
Figure 32- Iteration process 26
Figure 33- Optimization progress front panel. 27
Figure 34-Energy evaluation front panel. 27
Figure 35- Magnetic flux density field components. 28
Figure 36- B_z magnetic flux density component (Tesla). 28
Figure 37- Schematic of the characteristics to be optimize. 29
Figure 38- Magnetic flux density in order to diameter of the coil and the distance to magnet 29

Figure 39- Magnetic flux density variation in order to diameter of the coil and the distance to magnet. 30
Figure 40- Transducer all assembled. 31
Figure 41- Accelerometer response by the selected signal. 32
Figure 42- Power generated with 6 cm between top magnets. magnets. 33
Figure 43- Power generated with 5,5 cm between top magnets. 33
Figure 44- Power generated with 5 cm between top magnets. 33
Figure 45- Power generated with 4,5 cm between top magnets. 34
Figure 46- Power generated with 4 cm between top magnets. 34
Figure 47- Power generated when the central magnets rise by 3 mm. 35
Figure 48- Power generated when the central magnets drop by 1.5mm. 35
Figure 49- Power generated when the central magnets rise by 1.5mm. 35
Figure 50- Power generated when the central magnets drop by 3 mm. 36
Figure 51- Transducer transfer function. 36
Figure 52- Power generated with 6 cm between top magnets. 37
Figure 53- Power generated with 5,5 cm between top magnets. 37
Figure 54-Power generated with 5 cm between top magnets. 37
Figure 55-Power generated with 4,5 cm between top magnets. 38
Figure 56- Power generated with 4 cm between top magnets. 38
Figure 57- Power generated when the central magnets drop by 1,5 mm. 39
Figure 58-Power generated when the central magnets rise by 1,5 mm. 39
Figure 59- Maximum power generated at each distance. 39
Figure 60- Maximum generated power at each displacement. 40
Figure 61- Optimization process and resulting signal. 42
Figure 62- Measured and target vibration and EFM resulted. 42
Figure 63- Optimization process and resulting signal. 43
Figure 64- Measured and target vibration and EFM resulted. 43
Figure 65- Optimization process and resulting signal. 44
Figure 66- Measured and target vibration and EFM resulted. 44
Figure 67- Power generated by each vibration source. 45

Acronyms

Iot	Internet of things
LPWAN	Low-power wide-area network
RF	Radio Frequency
D	Diameter of the coil
DM	Distance to magnet
EMF	Electromotive force
DAQ	Data acquisition system
GPIB	General Purpose Interface Bus
DDS	Direct digital synthesizer

Acknowledgements

First of all, I would like to thank my supervisor, Professor Luis Filipe Soldado Granadeiro Rosado for the guidance, support, and feedback through the elaboration of this dissertation. I want to thank the Instituto de Telecomunicações for the conditions and materials provided for the completion of dissertation.

I would then like to express my gratitude to my five colleagues and close friends André Oliveira, Pedro Coutinho, Miguel Andrade, Markiyan Pyekh and Sara Soares for being always there to give advice and for all the fun moments during this journey.

Finally, I would like to thank a lot to the pillars of my life, without them it would not be possible. Mother, father, sister and girlfriend, thank you very much for the unconditional support.

Chapter 1 Introduction

1.1 Purpose and motivation

Internet of things (IoT) is defined by objects that are capable to transmit data over the internet or other networks and be programmed for certain applications. IoT devices are pieces of hardware, such as sensors, actuators, gadgets, appliances, or machines. These devices need batteries as power supplies, but batteries can be expensive, have great operational cost (once they need to be charged or exchanged), and are not environmentally friendly. Energy can be harvested from a wide variety of sources and an alternative to batteries is power the devices with the use of energy sources presented in environment like solar energy, thermal energy, wind energy, vibration energy, amongst others.

Currently, it is increasingly necessary to recover all the energy possible, both ecologically and economically. Vibration is an example of an energy source that is very unused, but with great potential. Handy and abundant vibration sources are not being used to generate energy, such as railway lines, human and animal movements, and all systems powered by engines, such as cars.

Energy harvesting is the process by which energy is derived from external sources, captured and stored for small, wireless autonomous devices. Vibrations present in the environment can provide energy that can be harvested to charge wireless sensors or produce electricity. There are already devices on the market that can generate energy from vibration, however they are still very expensive and little used.

This thesis aims to develop an induction-based energy harvesting transducer and its characterization understanding what instrumentation is needed to characterize it and measuring the power it can generate.

1.2 Objectives

The main objective of this thesis is to make an induction-based vibration energy harvesting transducer, characterize it, measure the power it can generate and test the availability of some vibration sources. To be able to achieve the final goal, the objectives until reaching the final solution are:

- Understand and explain the main vibration harvesting energy systems.
- Identify and characterize relevant vibration sources for personal and industrial LPWAN (Low-Power Wide-Area Network) connected devices.
- Research and explain the models for induction-based vibration energy harvesting transducers and identify the main constrains on the design of those devices.
- Illustrate the design and prototyping of an induction-based vibration energy transducer.
- Develop instrumentation to characterize the transducers and to emulate operational conditions when included on a IoT device.

1.3 Document's Organization

This document consists of 6 chapters, the content of which is described below.

Chapter 2 presents the state of the art, where several energy harvesting transducers are presented, such as piezoelectric, electrostatic, and electromagnetic. A review of already existent electromagnetic energy harvesting systems and some commercial solutions already on the market capable of harvesting energy through the vibration.

Chapter 3 presents the characterization setup. It presents the devices used, explains how they are manipulated and shows the software programmed to test and characterize the transducer.

Chapter 4 contains a brief study about the behaviour of the magnet and its magnetic field and a explanation how transducer was elaborated and its specifications.

Chapter 5 shows the results of testing and characterization the transducer in the two programs elaborated and some explanations of what happened in these tests is also presented.

Chapter 6 contains the main conclusions about the work produced in this thesis and the future work to be done to obtain better results.

Chapter 2 State of the Art

2.1 Energy Harvesting

Obtain large-scale harvested energy is possible through sources like wind or solar. However, to power a LPWAN device, small-scale energy harvesters working from radio waves, temperature differences, or mechanical vibrations may be enough.

The solar source has two different ways of converting solar light to large scale electrical energy. One way consists of concentrating de radiation from the sun to heat a working fluid used to drive a traditional generator like a gas turbine. The other consists of using the photon energy falling in a semiconductor elevating the energy state of an electron from the valance electron band to the conduction band, allowing an electrical current. This is the operating principle of photovoltaic cells [1]. Although the solar source manages to obtain a large scale of energy, it is also possible to obtain small-scale energy. The devices needed to obtain small amounts of energy, follow the same process as the large-scale ones, but with smaller dimensions. For example, a photovoltaic panel but with small solar cells [2]. The major drawback of using the sun to power LPWAN devices for personal or industrial use is to be needed solar exposure, which may not always be available mainly when devices are not installed permanently on a given location.

As with solar energy, the wind source is also capable of producing large-scale and small-scale energy through wind turbines and small wind turbines [3]. However, they have moving parts that are difficult to implement and maintain in LPWAN devices. Solar and wind sources have significant disadvantages of being a source of power for LPWAN devices. Thus, small-scale sources such as radio waves, temperature differences, or mechanical vibrations are the possible solution for the final goal

The process of harvest energy through temperature differences is based on the Seebeck effect, which consists on the generation of an electric potential difference between two conductors or semiconductors of different materials, with different temperatures. The output voltage is proportional to the temperature difference between the two materials' junction [4]. However, thermal sources are challenging to find, and although sometimes on industrial applications can be found, personal LPWAN devices rarely can access one.

Energy can also be obtained through stray radio frequency and an antenna. There are two approaches, broadband and narrowband. The broadband approach can harvest a more significant energy amount because it uses a large part of the frequency spectrum comparing with the narrowband approach that uses only a small part of the frequency spectrum. The quantity of energy harvested depends on the location where the antenna is; dense urban areas with the signals from TV transmitters, satellites, and cell phones increases the energy harvested [5]. To be applied to LPWAN devices, they must be in an area where there are many radio frequency signals, which is not always the case.

As the wind and sun sources are difficult to implement and thermal and RF (Radio Frequency) sources are challenging to use due to the characteristics of the environment in which they are easily applied, vibrations appear as an alternative. Vibrations exist in almost all environments and seem to be the correct energy source to power LPWAN devices.

Mechanical vibrations can be converted to electrical energy through a transducer. The transduction mechanism can be electrostatic, through a variation at a capacitance; piezoelectric, through a piezoelectric property which is when mechanical forces applied to specific materials result in an output voltage; and finally, electromagnetic that uses electromagnetic induction to produce energy.

2.2 Piezoelectric Transduction

A transducer is a device used to convert energy from one nature form to another. To occur transduction, the form of energy must change. In the case of piezoelectric transduction, the energy conversion can be from mechanical energy to electrical energy, or vice versa.

The piezoelectric transducer, represented in Figure 1, is a type of transducer that converts the electrical charges produced in some materials with a specific characteristic into energy. The material when subject to pressure or stress, generates a voltage. Typically, the vibration of the environment around the energy collection device is the cause of mechanical stress. The word "piezoelectric" is defined literally by electricity caused by pressure or stress. This phenomenon is called direct piezoelectric effect.

The converse piezoelectric effect consists at the reverse process, which is when the piezoelectric transducer converts electrical energy into mechanical strain energy [6]. However, the converse effect is not within the central theme of this thesis and only the the direct piezoelectric effect will be analysed more in-depth.

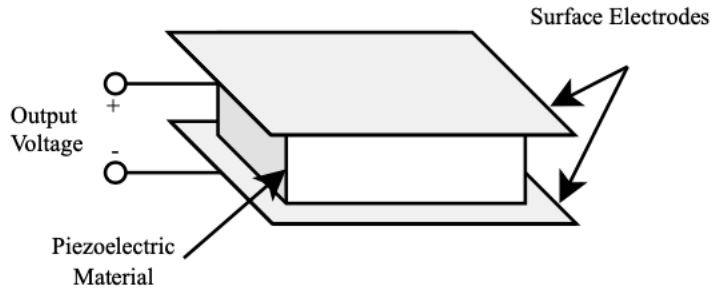

Figure 1- Piezoelectric transducer schematic.

The piezoelectric transducers have two standard coupling modes, the '33' mode, and '31' mode. The piezoelectric transducer pulsed an electric field in the '3' direction. It is the explanation of the first 3 in the name of the modes. The second number is the direction where the tensile or compressive force is applied. As presented in Figure 2, in the '33' mode, the force is applied along the poling direction, '3', and in the '31' mode, the material is strained perpendicular to the polling direction, '1' [7].

Typically, the '33' mode has a higher mechanical/electrical coupling factor than the '31' mode. However, when it is considered a very low-pressure source, the '31' mode conversion may have a more significant advantage in energy conversion. For a greater volume of piezoelectric materials, the '33' mode may be workable [7]. For instance, higher output energy can be achieved by increasing the

piezoelectric material layer with a stack configuration on '33' mode and stretching the piezoelectric element by bonding it to a substructure that undergoes bending on '31' mode.

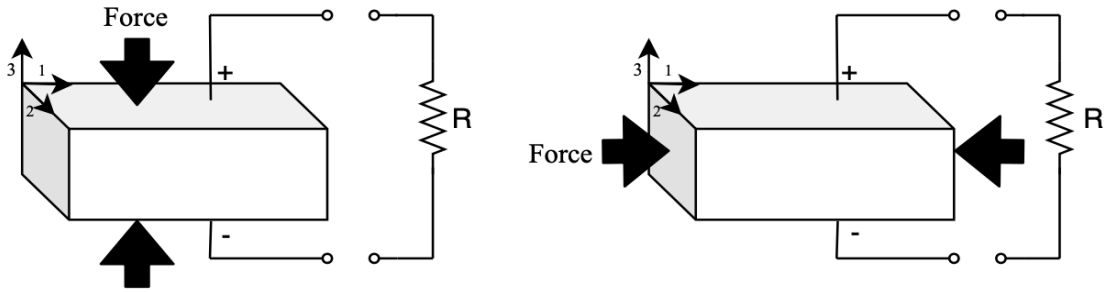

(a) (b)

Figure 2- Coupling modes for piezoelectric transductors: (a) '33' mode; and (b) '31' mode.

2.2.1 Piezoelectric Harvester Design

To obtain the best electromechanical coupling, many types of transducers were developed. However, the structures that use a free cantilever beam are the most usual. This structure consists of three main parts, the cantilever beam, the seismic mass, and piezoelectric layers.

The cantilever beam, Figure 3, is the basis of the structure and serves to amplify the relative displacement of the seismic mass to the vibration source's displacement amplitude. The seismic mass originates a higher output power because it increases the mechanical stress applied to the piezoelectric material. Finally, the active part of the structure, the piezoelectric layers that are used to convert mechanical vibrations into electrical energy [8].

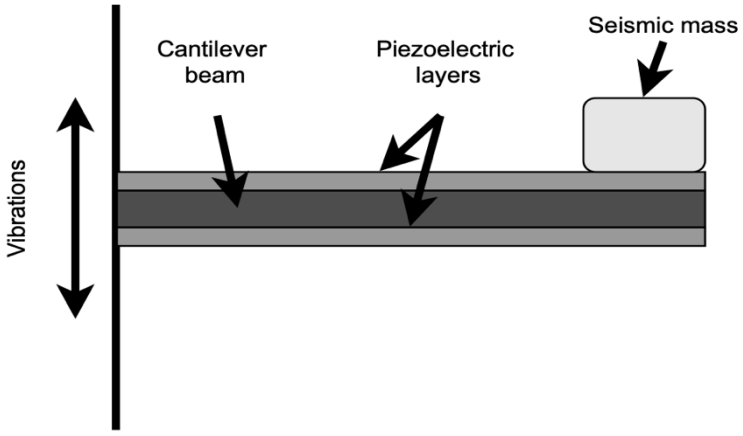

Figure 3- Basic cantilever beam energy harvester structure.

With the goal of increase the movement of the seismic mass and consecutively increase the impact on the piezo material and harvest more energy, magnets are added to the circuit. As can be observed Figure 4, the unique difference is the addition of four permanent magnets. Two magnets were fixed at the free end of the cantilever beam, while the other two magnets were fixed outside of the harvester's structure, near the other two permanents magnets, at the top and the bottom. The seismic mass movement, and the power harvested are increased by the repulsive and attractive force of the magnets [9]

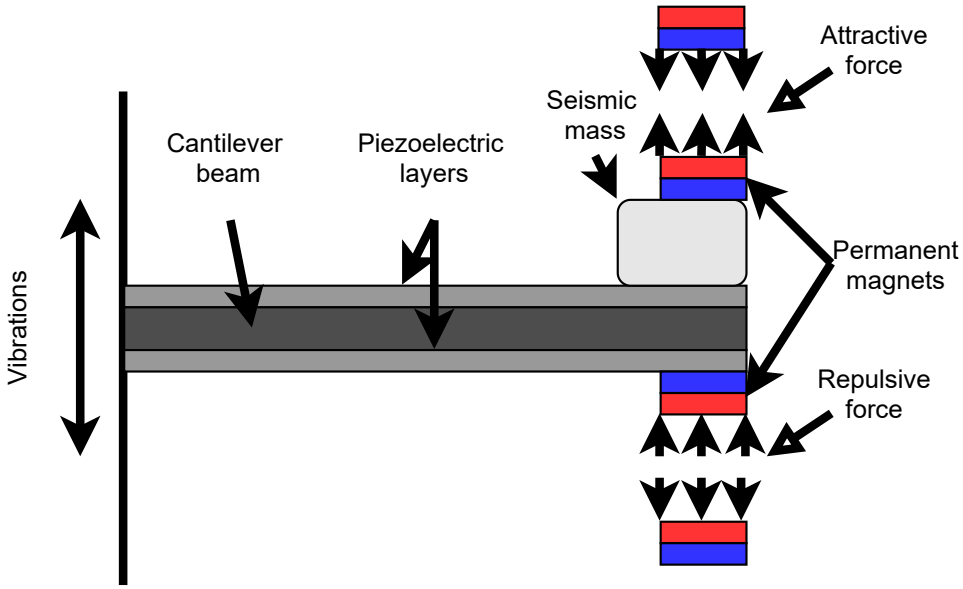

Figure 4- Cantilever beam energy harvester structure using permanent magnets.

2.3 Electrostatic Transduction

A capacitance structure made of two parallel metal plates separated by air, vacuum, or dielectric materials, also named capacitor, is responsible for the electrostatic transduction. A capacitance variation is generated when a relative movement between the two plates occur. Electric charges appear on the plates when there is a capacitance variation. There are two categories of these devices, electret free and electret based.

2.3.1 Electret free

Electret free electrostatic converters are passive structures that require an energy cycle to convert mechanical energy into electrical energy. Many energy cycles enable a conversion, but charge-constrained and voltage-constrained are the most common.

The charge-constrained cycle (Figure 5 and 6) is the most straightforward to implement on electrostatic devices. Only when capacitance reaches max value C_{max} (1) the cycle starts. The capacitor store an electric charge Q_{ctn} provided by an external source U_{min}. The device is then let in an open circuit (2), and when the structure moves mechanically to a position where its capacitance is minimal (3), the

capacitance C decreases and the voltage across the capacitor U increases because Q_{ctn} was kept constrained. Electric charges are removed from the structure (4) when the capacitance reaches its minimum (C_{min}) or when the voltage reaches its maximum (U_{max}) [10].

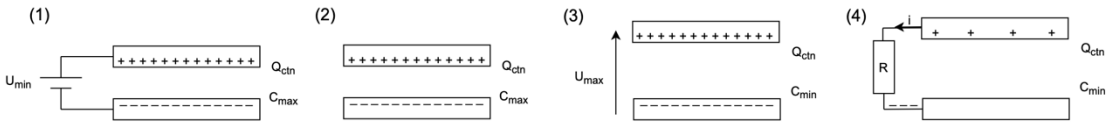

Figure 5- Charge-constrained cycle.

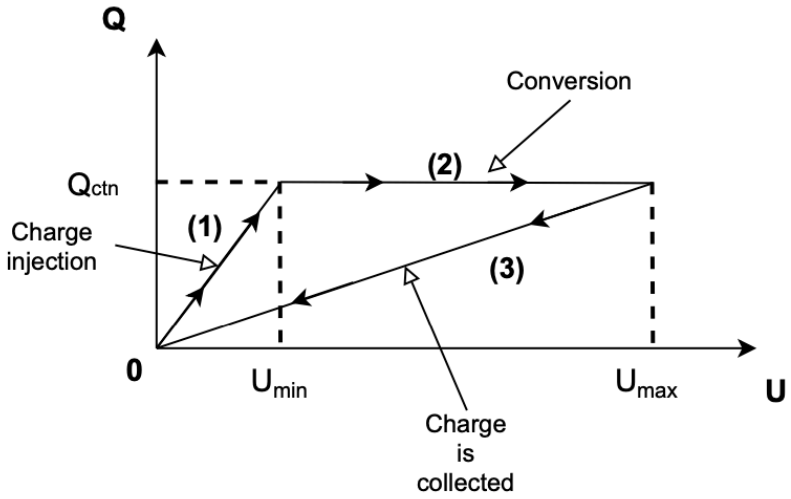

Figure 6- Charge-constrained cycle graph.

The quantity of energy harvested at each cycle can be obtained through the following formula

$$E = \frac{1}{2} Q_{ctn}^2 \left(\frac{1}{C_{min}} - \frac{1}{C_{max}} \right). \quad (4)$$

As the charge-constrained cycle, the voltage-constrained cycle (Figure 7 and 8) starts when the electrostatic converter's capacitance is maximal. The capacitor is polarized using a constant external power supply (1). The constant and external voltage applied, originate capacitance decreases, and the capacitor's charge increases, generating a current that is scavenged and stored (2). When the capacitance reaches its minimum value, the charge Q still presents in the capacitor is ultimately collected and stored (3).

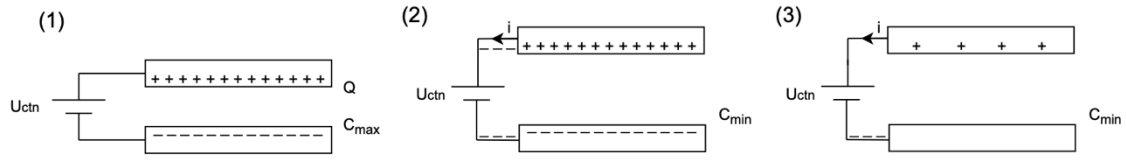

Figure 7- Voltage-constrained cycle.

The total amount of energy harvested at each cycle can be obtained through the following formula

$$E = U_{ctn}^2(C_{max} - C_{min}). \quad (5)$$

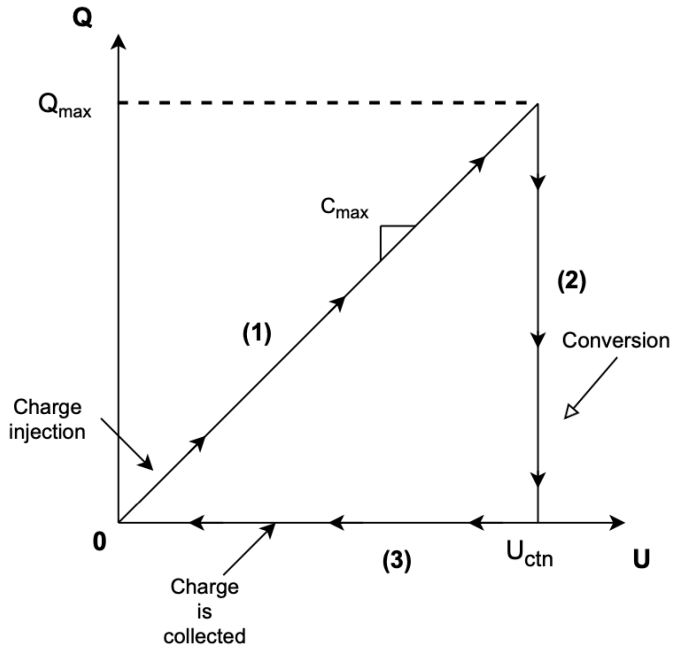

Figure 8- Voltage-constrained cycle graph

Both the charge-constrained cycle and the voltage-constrained cycle need an external power supply to polarize the capacitor to reach the maximum capacitance value. So, it is the biggest drawback of these converters. A possible solution to this problem will be the use of electrets that permit polarize electrostatic energy harvesters enabling a direct mechanical-to-electrical conversion and avoid any charge cycles.

2.3.2 Electret based

Electret-based electrostatic converters are very similar to electret-free electrostatic converters. The electret layers added on one or two plates of the variable capacitor, polarizing it. These characteristics are the main difference between the devices and enables its use without any external power supply.

Electrets are dielectric materials in a quasi-permanent electric polarization state that allows the flow of an electric current. They are electrostatic dipoles that can keep charges for years. This gives the converter the possibility of harvesting energy for years without any external power supply.

Some charge conduction phenomena may appear in electrets, modify their charge, and even make it disappear because dielectrics are not perfect insulators. An electret-based converter's lifetime is directly linked to its electrets' charge stability. Because of that, it is needed to apply stable ones to electret-based vibration energy harvesters.

The electret-based conversion device does not need any initial electrical energy to work. A structure deformation induces an output voltage directly, just like a piezoelectric material. The electret induces charges on electrode and counter-electrode, so the electret charges are distributed between electrode and counter-electrode. Therefore, the sum of Q1 (total amount of charges on the electrode) and Q2 (total amount of charges on the counter-electrode) is equal to the electret's charge, Qi, (Qi=Q1+Q2).

A relative movement between the counter-electrode and the electret and electrode induces a change in the capacitor geometry. When the counter-electrode moves away from the electret, the air gap changes, changing the electret's influence on the counter-electrode. It causes a reorganization of charges through load R (Figure 9) among the electrode and the counter-electrode. The relative movement between the counter-electrode and the electret and the electrode results in a current circulation through the resistance, R, and one part of the mechanical energy (relative movement) can be turned into electricity [10].

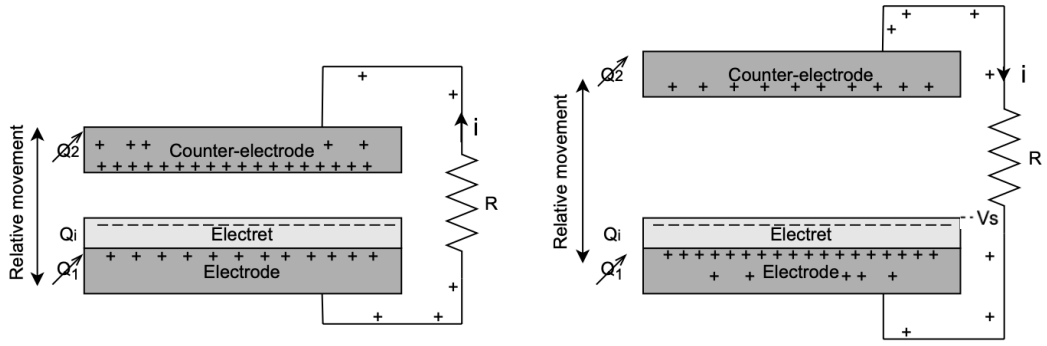

Figure 9 - Charge circulation of electret-based electrostatic conversion.

If at the terminals of the electret-based converter there is simple load resistance, the differential equation that characterizes the converter should be

$$\frac{dQ_2}{dt} = \frac{V_S}{R} - \frac{Q_2}{C(t)R}. \tag{6}$$

The output power of electret-based converter is directly linked with the surface voltage of the electret (V_s) and its lifetime is the lifetime of the converter, so it is essential that electret has a long lifetime to have a lasting electrostatic energy converter.

2.4 Electromagnetic Transduction

Electromagnetic induction is the basis of electromagnetic transduction. Electromagnetic induction happens when a conductor is placed close to a magnetic field, and the magnetic field continues to vary, or the magnetic field is stationary, and the conductor moves over the magnetic field. It is This phenomenon happens due to Faraday's law. This law relates the magnetic flux variation rate through a conductor (coil) to the electromotive force magnitude induced in that conductor [11].

Any electromagnetic transducer structure must have three items, a magnet, a coil, and a vibration source to make the magnet move. The magnet generates the magnetic field and the coil that is a conductor and finally, the most crucial part, the source that makes the magnet move. The relative movement between the coil and the magnet originate a magnetic flux variation that give rise to magnetic induction [12].

The spring has an essential function of absorbing external vibrations and consecutively make the magnet move regarding the coil. As shown in Figure 10, the magnet oscillates inside the coil according to the vibration source, inducing an electromotive force.

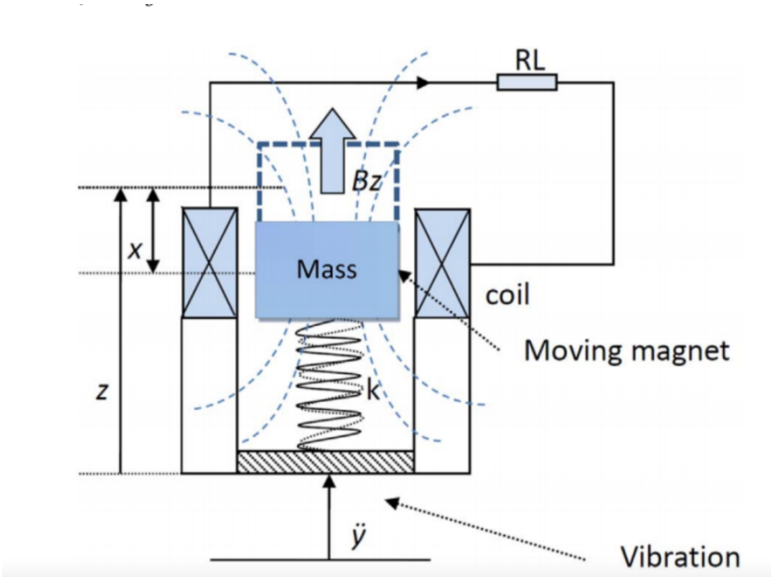

Figure 10- Model of an electromagnetic vibration transducer [12].

The electromotive force's amplitude is proportional to the moving mass's displacement speed (magnet) relative to the coil. This relative oscillating motion causes a varying magnetic flux inside the coil, and Faraday's law can determine the electromotive force induced in the coil through

$$\varepsilon_v = -\frac{d\Phi_B}{dt} \tag{7}$$

where Φ_B(Weber) is the magnetic flux and ε_v (Volt) the voltage induced.

To improve the characteristics and increase the values of energy harvested, other designs have been developed and will be presented and explained below.

2.4.1 One-Magnet Spring-Based Electromagnetic Energy Harvester

The one-magnet spring-based Electromagnetic Energy Harvester is a design that brings better results. As shown in Figure 11, it is constituted by a non-metallic cylindrical structure that contains one magnet and two helical springs, one connected to the top of the magnet and top of the structure and the other connected to the bottom of the magnet and bottom of the structure. To be able to harvest the energy, there is also a coil around the magnet outside the structure.

Due to an external vibration source, the helical springs absorb the vibration, causing the magnet to move through the coil and consequently alter its magnetic flux, inducing a voltage in the coil [13].

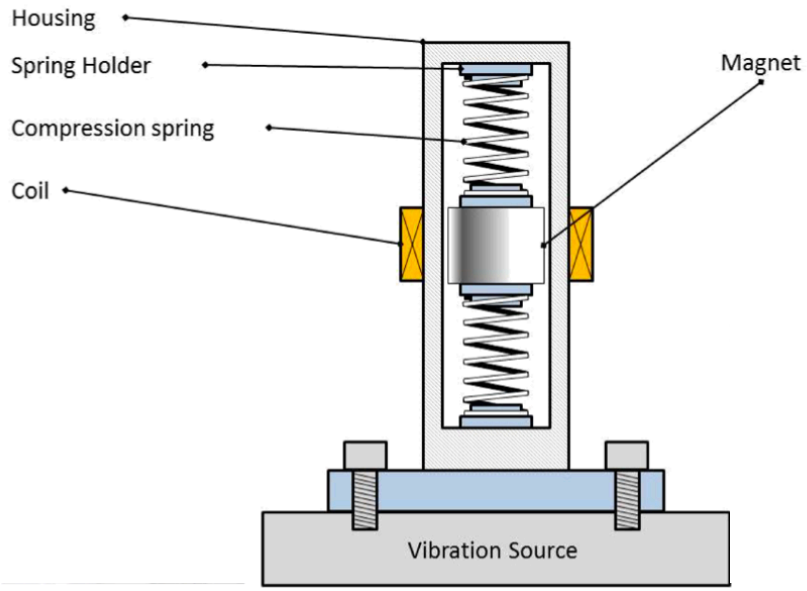

Figure 11- One-Magnet Spring-Based Electromagnetic Energy Harvester design [13].

The top spring eliminates the gravitational force effect acting on the magnet. Compared to the previous example, the oscillations of this topology have less damping effect. However, this vibration energy harvester device has a significant disadvantage. The springs bring to the harvester device the buckling effect resulting from the sudden change in the spring's shape under a load (deformation). It makes the springs to consuming part of vibrational energy and its damage. This lead to a system performance degradation over time.

2.4.2 Flux-guided Magnet Stacks Electromagnetic Energy Harvester

Flux-guided Magnet Stacks Electromagnetic Energy Harvester is based, as presented in Figure 12, on a non-metallic cylindrical structure that contains two generators and a free inertial mass, responsible for inducing current at the generators. There is a generator located at each side of the apparatus. Each

generator is composed of a helical spring connecting the top or bottom of the structure to the magnet, and each generator has a coil around the magnet outside the structure.

The freely movable inertial mass is a non-magnetic metal ball responsible for making the magnets move, generating electrical energy. It needs a specific motion source to the inertial mass hit at the magnet with the maximum inertial energy to obtain the maximum energy harvesting.

The impact of the inertial mass results in springs vibrations, and generators transfer the mechanical energy into electrical energy under electromagnetic induction [14].

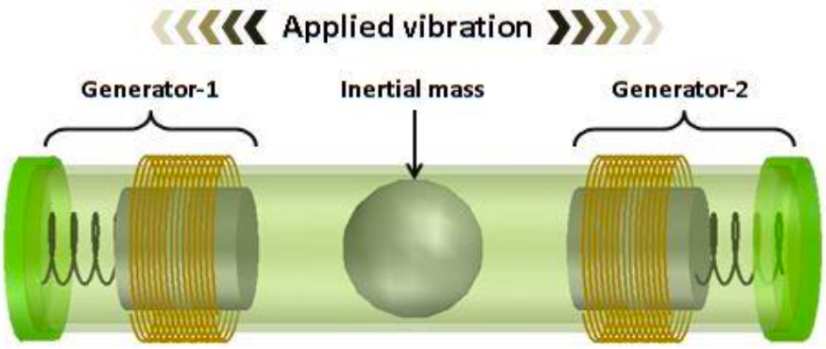

Figure 12- Flux-guided Magnet Stacks Electromagnetic Energy Harvester design [14].

The principal handicap of this electromagnetic energy harvester is that the motion's source must be efficient and specific (arrows direction). Only like that, the mechanical force applied to the magnet will be the maximum to obtain the maximum electrical energy. The inertial mass impact on the magnets will be damaging the mass and the magnets over time and as the one-magnet spring-based electromagnetic energy harvester presented above, the use of springs has the disadvantage of the buckling effect's appearance.

2.4.3 Magnetic Levitation Vibration Energy Harvesting Transducer

Considering the disadvantages that the springs bring to the electromagnetic energy harvesters, a device that avoided its use was proposed. It is also essential to make the vibration sources nonspecific and the harvester could be implemented in several situations and locals.

Maglev electromagnetic harvester is based on the levitation phenomenon. As can be seen in the Figure 13, the magnetic levitation harvester consists of two magnets, one on the top and the other on the bottom, mounted inside a cylindrical non-magnetic tube. The fixed magnets are levitating the third magnet because each magnet pair with magnetic poles oriented to repel causes the levitation force. The coil is situated outside the tube, around the levitation magnet. Air compressively attenuates the

levitation magnet's movement, so holes were made on the tube to solve this situation. External vibrations on the tube originate oscillations on the moving magnet and magnetic flux changes [15].

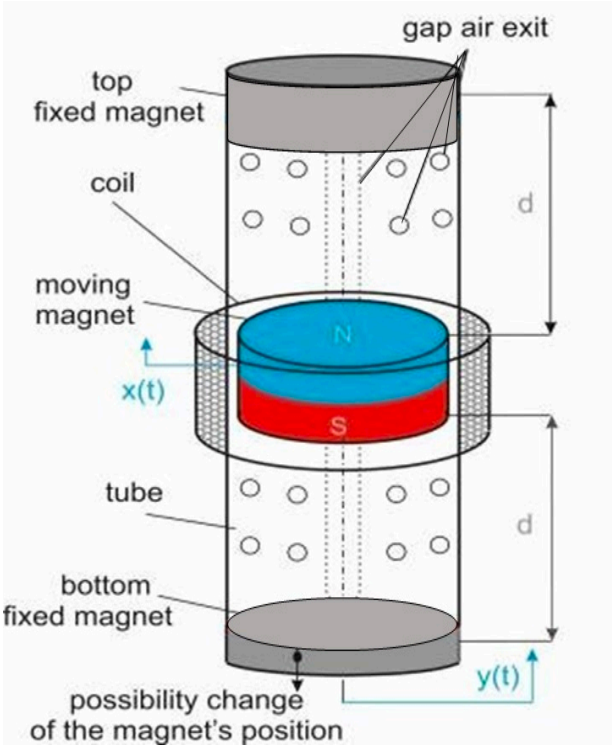

Figure 13- Maglev Electromagnetic Energy Harvester design [16] .

2.5 Commercial Solutions

There are already some examples of vibration energy harvesters on the market that suit the initial objectives of this thesis. In this section will be present some of them.

2.5.1 HIPER-D

Hiper-D device produced by the Kinergizer company, converts ambient motion to electricity when set up in a motion source and it has the capacity to generate up to 89 mW of power. This device has a case made of rigid plastic, weighs 90 grams, and is waterproof. However, it cannot be used anywhere, it has some specifications. A motion source must have a vibration smaller or equal to 5g and a frequency between 2 and 200 Hz. The device and the amount of power that this device can generate depending on the frequency and the vibration source can be seen in figure 14. Unfortunately, the commercial price of the device wasn't available to the public.

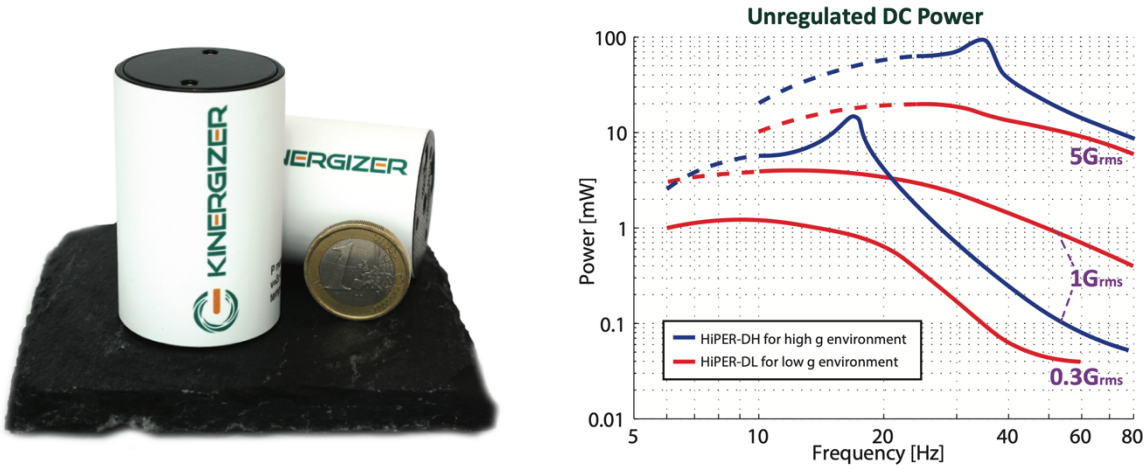

Figure 14- Hiper-D transducer and its characteristics.

2.5.2 ModelC

ModelC (Figure 15) is one of the devices produced by the company ReVibe Energy. As in the example above, it is also designed to produce electrical energy from vibration. Nevertheless, this one with the specificity of having a shorter source frequency range, from 10 to 30Hz, and a big vibration acceleration range with 0.05 to 10g. Its output is available AC and DC; it can generate power between 0.5 to 150mW and dimensions of 80 x 50 x 25 mm. This device has a price of €295.

Figure 15- ModelC transducer.

2.5.3 ModelD

ModelD (Figure 16), also from ReVibe Energy, is the one that can generate the highest power output; it is also the model with some vibration source requirements most common to find. With a frequency range of 30 to 150Hz and vibration acceleration range of 0.05 to 2g. It has dimensions of 63 x 33 mm and it can generate power since 0.5mW to 200mW. It also has the characteristic of both AC and DC output available. The price of this device is €645.

Figure 16- ModelD transducer.

Chapter 3 Characterization setup

One of the objectives of this thesis was to analyse the transducer and its behaviour to optimize it. In the absence of a setup capable of analysing it, the priority was to build a setup that allows the control and careful analysis of the transducer. To analyse the transducer, it was necessary to generate a stimulus that would make it vibrate and connect it to a source of vibration. This source was necessary so that the magnetic induction phenomenon caused by the relative movement between the magnet and a coil that is part of the transducer creating an EMF could occur.

As observed in Figure 17, the characterization setup was composed of an instrumentation block, whose architecture will be explained below. The instrumentation block provided the vibration stimulus to the transducer and acquired the EMF generated by the transducer. Furthermore, the instrumentation block interacted with a computer with a LabVIEW software responsible for processing and controlling data received and sent.

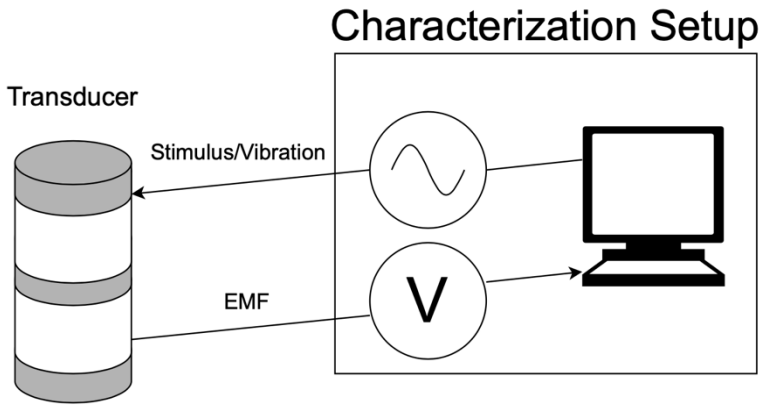

Figure 17- Characterization setup interaction with the transducer.

3.1 Architecture

The instrumentation architecture block was designed to meet the processing and control needs required to achieve the proposed objectives. Knowing that the presence of a vibration source where the transducer would be applied is needed, the first task was to decide which vibration source to use. The choice was the Vibration Generator 2185.00 that vibrates according to the wave introduced at the input terminal. This wave was provided by the TG1010A Programmable 10MHz Direct digital synthesizer (DDS) function generator, programmed by General Purpose Interface Bus (GPIB). However, the function generator did not provide enough power for the vibration generator to work, so a power amplifier had to be added to the system, along with a voltage source required by it.

Once the vibration generator was working, the need was to measure the amount of vibration generated in each imposed signal, so an accelerometer was introduced in the system. The accelerometer was coupled to the vibration generator through the coupling system. The data were acquired using a data acquisition system (DAQ).

The transducer, which was coupled to the vibration generator, generates an electromotive force when in operation. To be able to measure the power generated by the transducer, it was necessary to apply the electromotive force to a load resistance. The load resistance simulates the power system by the generated power. The load resistor terminals also connect to the DAQ so that generated energy could be measured and analysed. Load resistance was also programmed by GPIB by a Programmable Resistance Substituter.

The setup system that allows analysing the transducer and processing its data can be seen in the Figure 18.

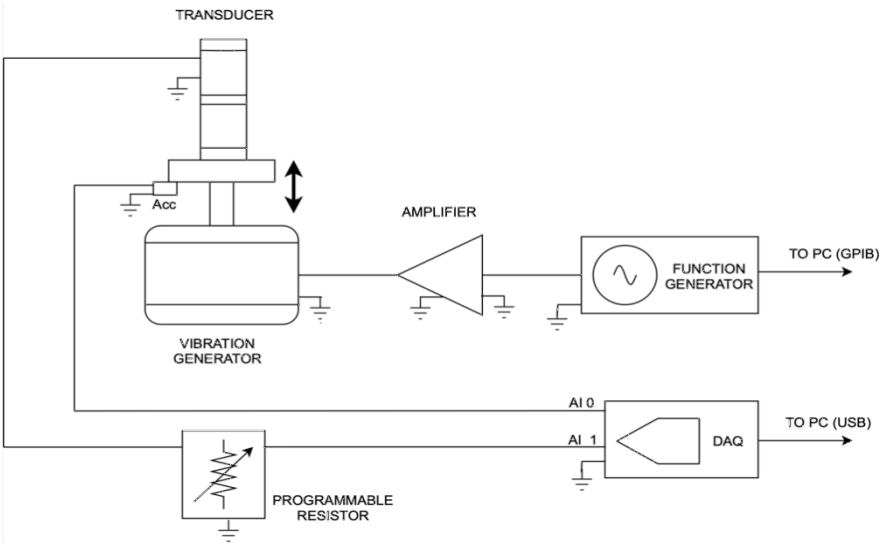

Figure 18- Characterization setup.

3.2 Vibration Generator and Transducer Coupling Mechanism

As mentioned above, to test the transducer, it was essential to use a source of vibration. Sources already present in nature or in everyday life could have been used, such as the collar of any animal that moves, a train rail, or a washing machine in operation. However, the Vibration Generator 2185.00, showed in Figure 19, because it is a more practical option that would allow testing the transducer in a laboratory environment.

Figure 19- Vibration generator 2185.00.

The 2185.00 vibration generator has the advantage of being very versatile and be ideal for waves experiences since it vibrates depending on the wave applied to its inputs. It operates like a loudspeaker essentially, characterized by a coil wound in a thin aluminium tube that moves relative to a permanent magnetic field when a current from the wave imposed on its inputs is applied.

The vibration generator also had specifications that meet the needs of the waves tested. It had a frequency range from 0.1Hz to 5Khz and a maximum current of 1A, limited by a fuse.

Once with the chosen vibration source, it was needed to couple the transducer to the vibration generator. Since the tap centre with the banana was the only part of the transducer that vibrated, the transducer had to be attached there, so the solution found was to design and produce parts in a 3D printer to solve the problem found. First, the base part that fit the banana and then an intermediate piece where the transducer was connected that fits the base part, as shown in Figure 20

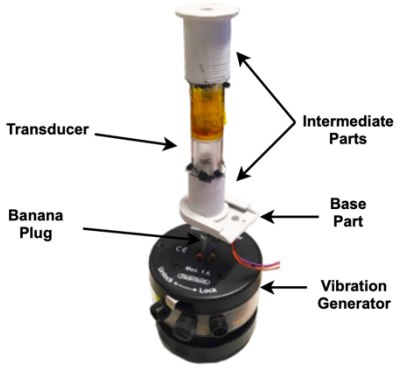

Figure 20- Printed parts connections.

The base part was designed to fit the banana plug and to be installed on it the accelerometer, so that the accelerometer could measure the amount of vibration generated as can be seen in the Figure 21.

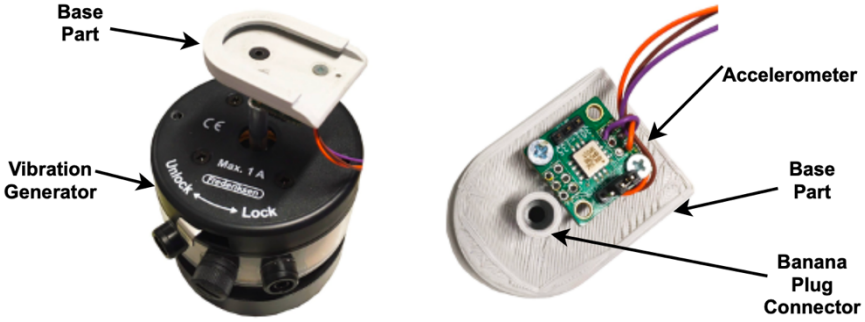

Figure 21- Base part connections.

It also allowed the intermediate piece, that connects to the transducer, to fit in it and allowed connecting and disconnecting to test the various transducers. The intermediate part was connected to the transducer through hot glue. The intermediate part connections can be seen in the Figure 22.

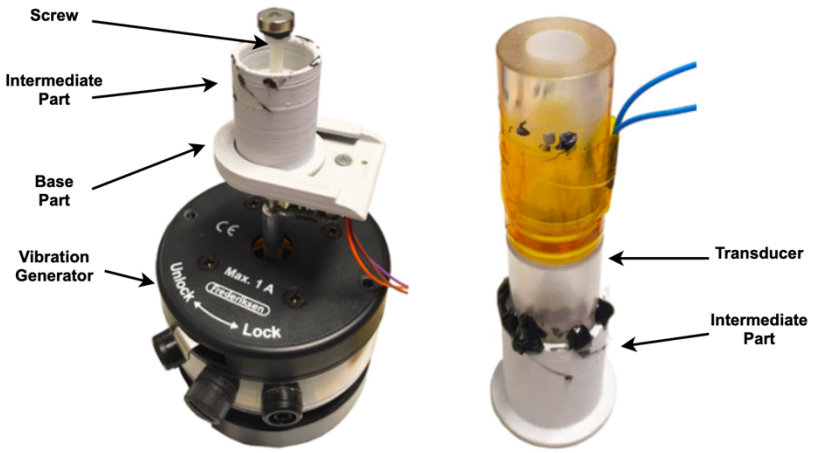

Figure 22- Intermediate part connections.

This part had a fundamental particularity which is allowing introduce to the transducer design the possibility of moving the extremities magnets trough a screw installed on this intermediate part, as is shown in the Figure 23. The top magnets were connected to the screws trough hot glue.

Figure 23- Screw installation.

After all this was set, the next task was to generate and apply the wave to the vibration generator terminals, discussed below.

3.3 Signal Generator

The operation of a vibration generator is dependent on a signal imposed on its terminal inputs, as explained above. Then we needed to introduce a function generator into the system, so the Programmable 10 MHz DDS Function Generator TG1010A was used, which was available in the laboratory. This function generator can generate waves programmatically through the GPIB protocol.

For more convenience and speed to change wave parameters during tests, it was necessary to configure the wave programmatically. A Labview software was used to control the wave programming.

Initially, the Labview software was able to program sine, triangular, and square waves and their frequency and amplitude. These waves applied to the vibration generator gave rise to vibration and, in turn, the operation of the transducer and its analysis. However, to have an accurate idea of the amount of energy that the transducer could generate, it was necessary to apply it to everyday life vibrations sources, which was not the case with sinusoidal, square, and triangular waves. Then the ability of the function generator to generate arbitrary waves was added to the program. This characteristic of the function generator created the possibility to test the transducer on accurate vibration sources such as a moving car or a bridge.

However, the wave produced in the function generator has a very limited current capability, insufficient to make the vibration generator vibrate, so it was necessary to amplify it. So, an audio amplifier was needed to bring to the system. By requirement of the audio amplifier M033N which was introduced, it was also necessary to bring to the system a voltage source.

The part of the characterization setup responsible for getting the transducer to work was complete upon completing this task.

3.4 Data acquisition

With the transducer working, it was necessary to analyse the data coming from it. The first to analyse was the vibration coming from the vibration generator for any imposed wave. So, first was added the ADXL337 Breakout accelerometer to the coupling mechanism, but its range was only +- 3g, and with some imposed waves, the accelerometer saturated. Then it was replaced by the ADXL357 accelerometer, shown in Figure 24, which allowed selecting the acceleration range between +-10g, +-20g and +-40g through a switch. After some measurements, the range of +-10g was selected as it was sufficient for the vibrations to be measured.

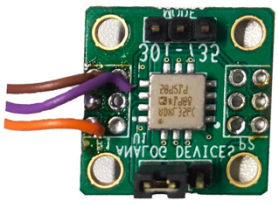

Figure 24- ADXL337 accelerometer.

To be able to measure the power generated by the transducer, it was necessary to introduce a load resistance to the terminals of the electromotive force generated so that current could pass through the resistance, and it was possible to analyse the generated power. As the load resistance impedance influences the generated power, a Programmable Resistance Substituter, presented in the Figure 25, was introduced in the system, which allowed us to adjust the load resistance value and see the resistance value for the maximum power.

Figure 25- Programmable Resistance Substituter.

A data acquisition system (DAQ), the USB-6009 from Nacional Instruments, Figure 26, was used to acquire the generated power and the accelerometer signals because it can acquire signals and is compatible with the analysis and processing program developed in Labview. This DAQ provides eight single-ended analog input (AI) channels, two analog output (AO) channels, 12 DIO channels, and a 32-bit counter with a full-speed USB interface.

Figure 26- USB-6009 DAQ.

3.5 Processing and control software

In the project planning, the need to have a component for processing and controlling the system devices arose. This was necessary for testing and improving the transducer. Considering the devices used and their purpose, the most practical and most accessible option to implement the processing and controlling component was the LabView software from the National Instruments (NI) company because it is enabled with native GPIB interface libraries and DAQ support, beside all the signal processing functionalities.

The software development evolved as the devices were introduced into the system and had two versions, an initial version to characterize the transducer, and the second to test the transducer with emulated sources of vibration.

3.5.1 Transducer Characterization

The first version to characterize the transducer test the operation of all devices with a sinusoidal, square, or triangular periodic wave and the second version where the waves that are imposed on the vibration generator emulate vibration sources.

The front panel of the initial version is shown in Figure 27 and can be consulted the different parts of it. This initial version was responsible for the control/processing of the devices of the system.

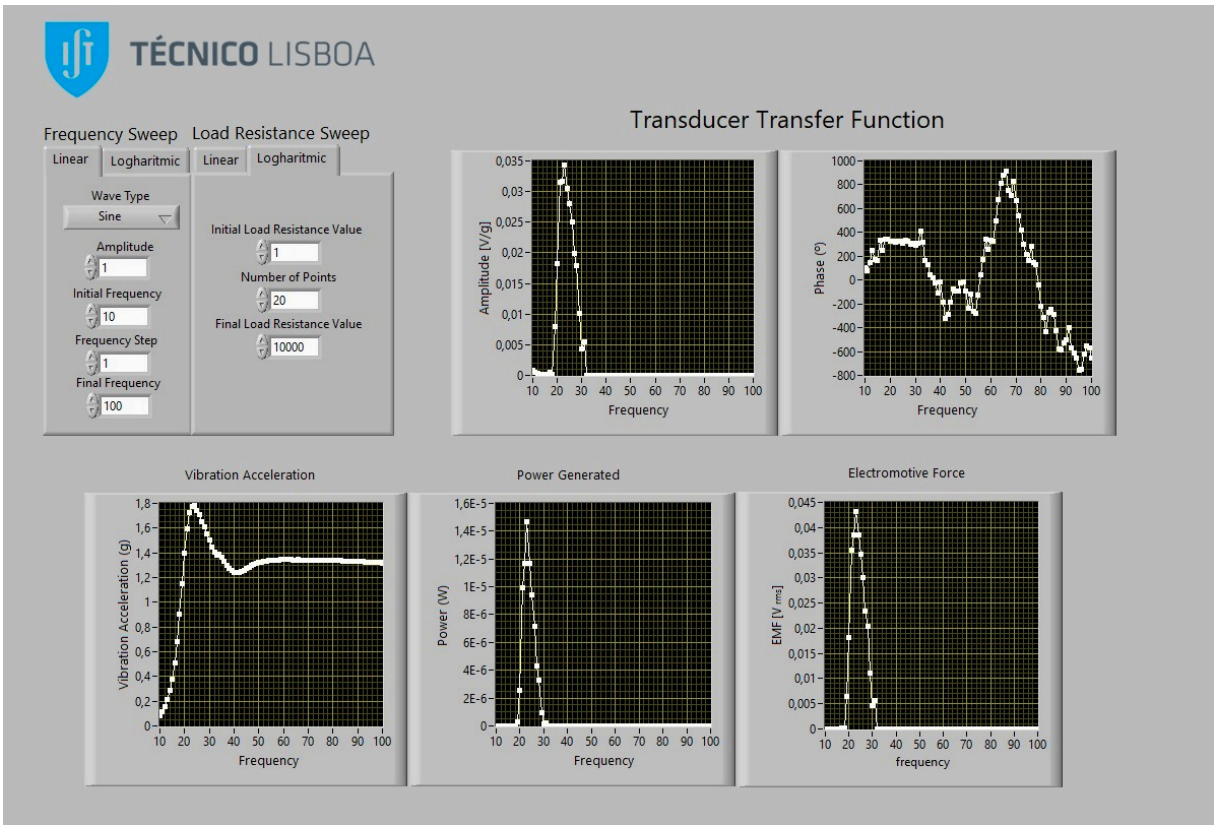

Figure 27- Transducer characterization front panel.

In the frequency sweep block is shown the part responsible for selecting the characteristics of the wave to be programmed in the function generator. The function generator output wave was chosen in the program between sinusoidal, square, or triangular waves as well as their amplitude. The program also allowed frequency sweeps, selection of the start and end frequency and the type of sweep to be performed in the program. The sweep can be linear or logarithmic, selecting the frequency step in the linear case and the number of points in the logarithmic case.

The load resistance sweep block represented the part that program the load resistance applied at the output terminals of the transducer. The program simultaneously maked load resistance sweeps, linear and logarithmic, selecting the initial and final load, the step, and the number of points, for the linear sweep and the logarithmic sweep, respectively. The program was designed to allow compatibility of both sweeps, for each load resistance value, a complete frequency sweep was carried out.

Regarding the signals acquired by DAQ, their processing can be consulted in the represented graphs. The vibration acceleration graph shows the fundamental component of the vibration acceleration generated at each frequency. This graph was achieved by acquiring the signal coming from the accelerometer installed in the vibration generator. Acceleration is displayed in units of g, but information from the accelerometer comes in Volt. The conversion was done by checking the accelerometer's sensitivity and dividing the voltage coming from the accelerometer by its sensitivity.

The power generated graph shows the power that the transducer can generate at each frequency at a given load resistance value. The graph was achieved by acquiring the fundamental component of EMF signal, which was squared and divided by the load resistance in the program to display the power value.

The transfer function of the transducer graph is also represented. The amplitude graph was obtained through the division of the output signal (EMF) by the input signal (vibration acceleration). The same procedure was done in the phase graph, but instead of dividing, the phase of the output signal was subtracted from the input signal. The transfer function was important to see the influence of the vibration acceleration in the EMF generated.

Although the data collected and presented were interesting and showed how the transducer works, they had no practical foundation, as the vibration used did not simulate a source of vibration to which the transducer could be applied.

3.5.2 Evaluation of Emulated Vibration Sources

The second version of the program emerged from the need of testing the transducer on known and real vibration sources.

To the system be able to simulate the characteristic vibration of a real vibration source, it was necessary to apply a wave to the system input that gave rise to that same vibration source. The objective would be to find which wave apply to the input system so that the vibration generator simulates the characteristic vibration of these vibration sources after the influence of the system.

The model characterization tab of the program was elaborated to know the influence of the system on a signal that passes through it, whose front panel can be seen in Figure 28.

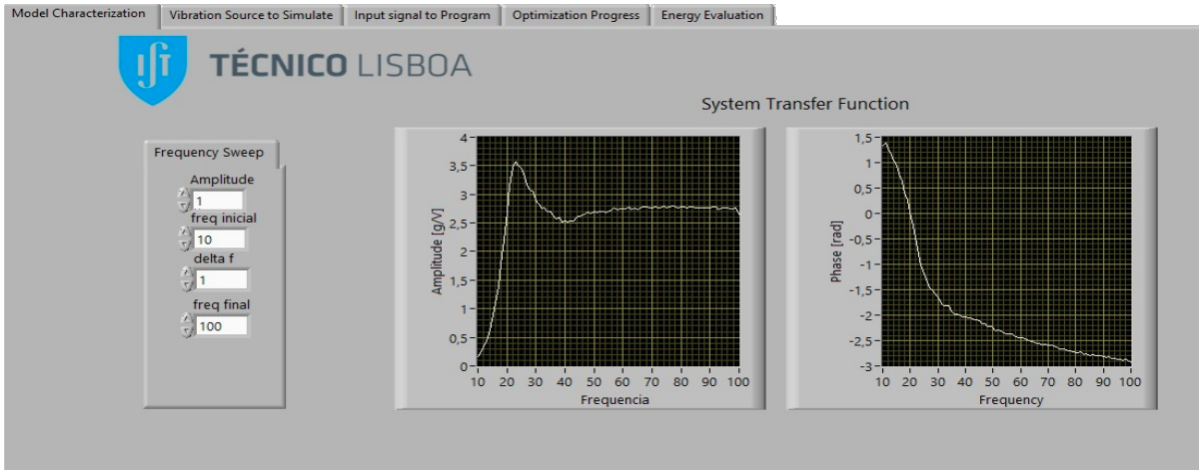

Figure 28- Model characterization front panel.

The system was characterized by a frequency sweep of a sine wave because it was the only wave that does not have harmonics, thus being a more accurate characterization of the system.

The system could only generate frequency response above 10 Hz, a limitation of the stimulation chain (signal generator + amplifier + vibration generator) in particular of the audio amplifier because it behaved like a high-pass filter, because of the output decoupling capacitor. By restriction of the acquisition board, the system was limited to 100 Hz. So, the characterization of the model was limited to between 10 and 100 Hz.

Knowing the influence of the signal imposed on the system, it was now necessary to analyse the vibration of the required sources. As it was impossible to measure the vibrations directly from the sources, the Energy Harvesting Network Data Repository was consulted, which contained data of the following vibration sources as a function of time and was downloaded [17]. The data downloaded were from the following sources seen in the Figure 29.

a) Engine of Ford Focus. b) Water pump motor. c) Low leg.

Figure 29- Vibration sources chosen to simulate.

On the engine of 1999 Ford Focus 1.6 Petrol, Figure 30a, the accelerometer was placed in a plate bolted onto the engine during a trip. In the second case the accelerometer was placed at a motor of district hot water circulating pump, Figure 30b. And third source was collected through an accelerometer attached to a men's ankle as can be seen in the Figure 30c. The data logger was tied to the body using self-adhesive support bandage rolled on under tension. The tests were carried out at a medium speed of 3.5 km/h.

This repository was created to provide an open source for sharing vibration data and it was authored by the University of Bristol and Southampton [17]. After downloading the data from the repository about the vibration sources, it was necessary to take care of the data to be used and processed. For this purpose, a MatLab program was created to receive and edit the file with the vibration data. This program standardized all the data to be received in the Labview software. The result of the second part of the second version of the program is shown on the Figure 30.

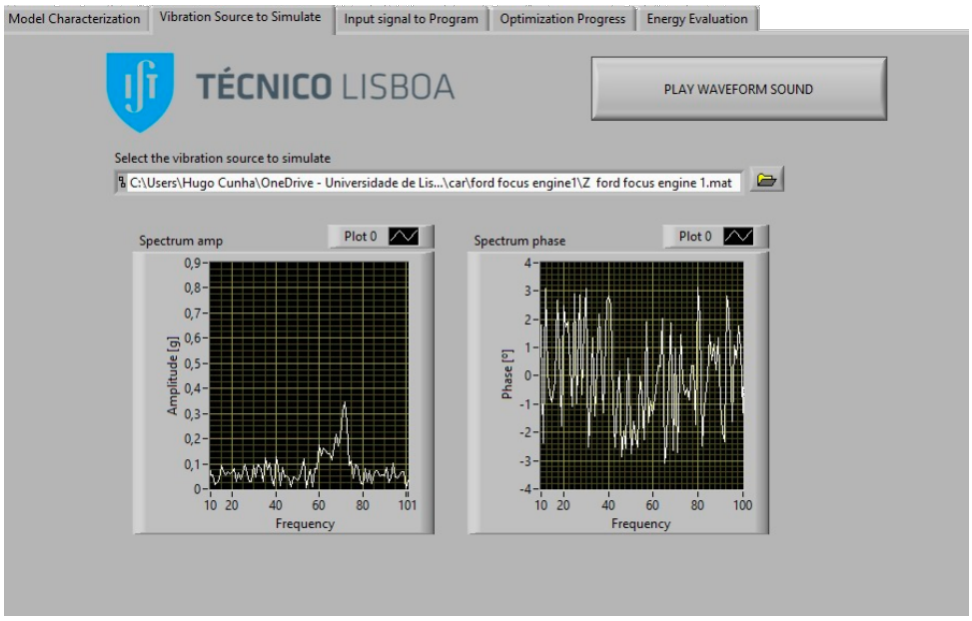

Figure 30- Vibration source to simulate front panel.

This second part is responsible for choosing the vibration source to simulate in the vibration generator and for processing its data through selecting the file containing the data of a specific vibration source. This data, coming from the repository mentioned above and previously treated in MatLab, came in units of g and as a function of time. This data was crucial because it allowed finding the wave to be programmed in the function generator. However, the characterization of the model was as function of frequency, so it is necessary to apply the Fast Fourier Transform (FFT) to the chosen signal to agree with the characterization of the system and the FFT spectrum result can be seen in the Figure 31.

Since the model's characterisation and the system's output at each frequency were established, the next step was to find the wave to impose at the function generator, the input of the system. Part 3 of the program was responsible for calculating the signal imposed on the input and programming it in the function generator. Having characterised the output signal as a function of frequency and knowing the transfer function of the system, maked possible to calculate the signal at the input of the system, as can be observed in equation 8,

$$X(f) = \frac{Y(f)}{M(f)}, \tag{8}$$

being X the input signal, Y the output signal which means the data of the vibration source to simulate, and M is the model characterization. As the model is limited to frequencies between 10 and 100 Hz, to calculate the signal to introduce at the system's input, the output signal also had to be restrained from 10 Hz to 100 Hz. The input signal was achieved by dividing the output signal by the transfer function.

After having accessed the input wave, the next step was to program it in the function generator, and for that, we used the function present in the function generator to program an arbitrary wave. This programming was achieved through the GPIB interface and had the characteristic of receiving precisely 1024 points, each with a value in the range -512 to +511, i.e., 10-bit vertical resolution.

Figure 31 shows the front panel of the 3rd part of the second version of the program, in which the wave is programmed.

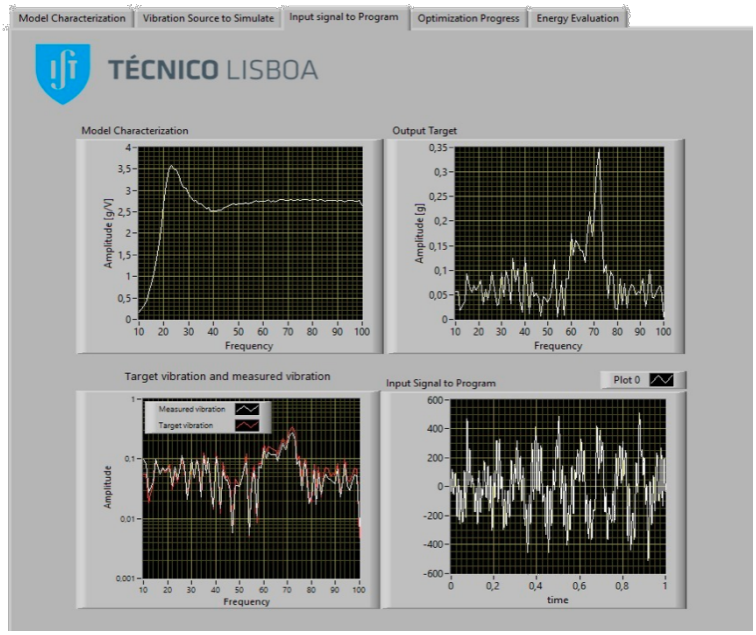

Figure 31- Input signal programming front panel.

It can be observed in the Figure 31 the model characterization, the output target, which is the vibration data downloaded, the signal that was sent to the function generator to program the input signal, and also can be observed the vibration target and the respond to the signal programmed at the output, the vibration measured.

As can be seen, the programmed signal originates an output signal that still had some differences with the target signal, so the need arose to obtain a signal closer to the intended one. For this purpose, the optimization process tab was created, responsible for approaching the output signal to the intended signal through iterations made according to the scheme in Figure 32.

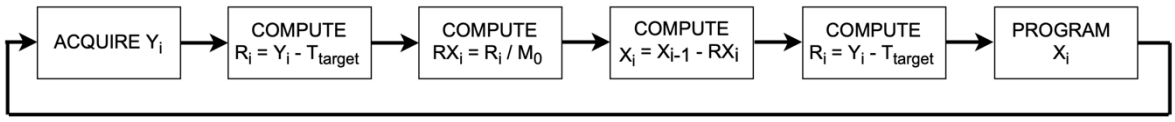

Figure 32- Iteration process.

Where Yi is the signal measured by the accelerometer at each iteration, Y_{target} is the target signal, R_i is the residual value of the iteration, M0 the model transfer function, RX_i is the residual input value, X_{i-1} is the programmed signal (input signal) in the previous iteration and X_i the signal to program in the current iteration.

The front panel of optimization process tab that can be observed in Figure 33 consists of the graphs of the signal of the measured vibration and the intended vibration overlapped, the graph of the summation of the differences of the same signals to see if the iterations bring the signals closer, and the

graph of the output signal resulted of each iteration programming. The summation of the differences between measured and target signal was achieved through the equation

$$D_i = \sum M_i(f) - T(f), \quad (9)$$

being M_i the measured vibration at the vibration generator at each iteration, T the vibration target and D_i the summatory of the difference between the measured and target signal at each frequency.

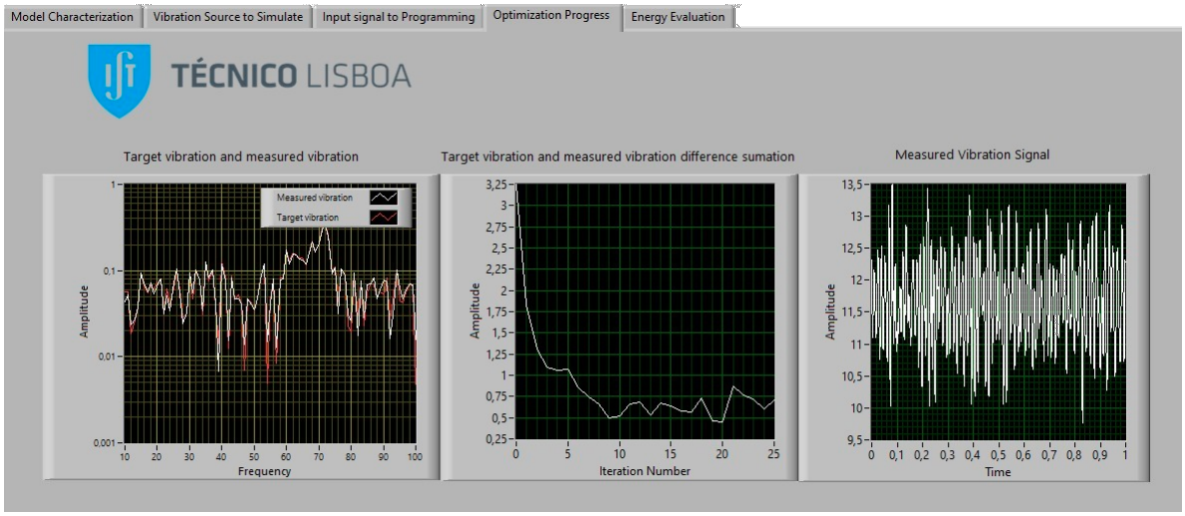

Figure 33- Optimization progress front panel.

After making the necessary iterations and achieving the output signal as similar as possible to the target signal, it is now necessary to test the transducer on an authentic vibration source simulated.

The fifth tab of the program, Figure 34, presents the electromotive force and the power generated by the transducer applied to the simulated vibration source varying the load resistance as wished. The load resistance values were selected in the load resistance sweep and could be selected a linear or a logarithmic sweep. Still, it can be observed in the Figure 34, the power generated by the load resistance sweep selected and the electromotive force spectrum in the frequency range that the system can generate.

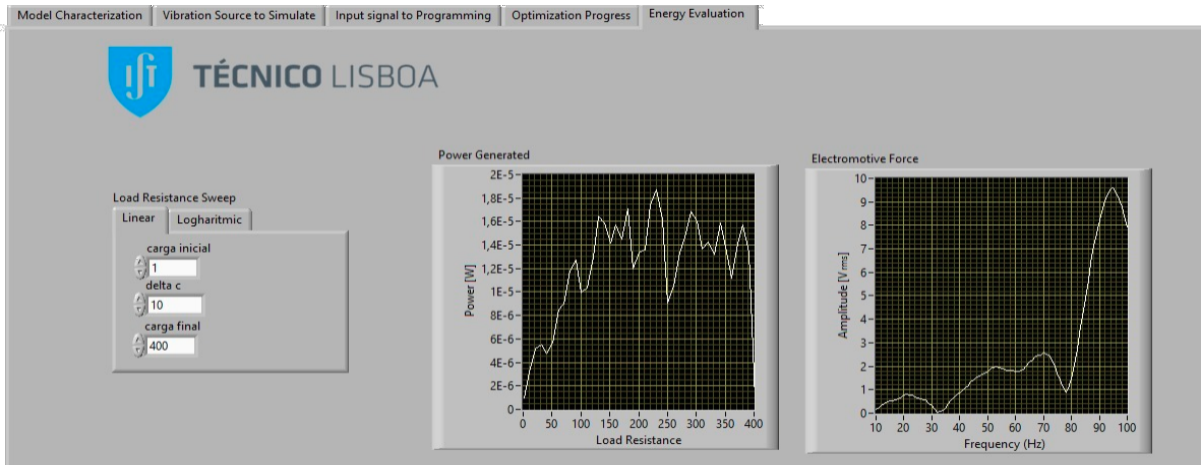

Figure 34-Energy evaluation front panel.

Chapter 4 Transducer Design

According to the theory, the electromagnetic transducer consists of a magnet, a coil, and the relative movement between them. The location and dimension of the coil regarding to the magnet is essential to maximize the energy harvesting process. So, to develop the transducer, it will be necessary to study the behaviour of the magnet and its magnetic field to place a coil in the most suitable site. For this, a simulation of a magnet's magnetic flux density simulation based on a script in *MATLAB* that allowed the computation of the 3D field coordinates of the magnetic flux density of a magnet was performed. The magnet used was characterized by a magnetization of $1x10^6$ A/m, 11mm of diameter and 5mm of height. The script was downloaded from the repository *GitHub* which its author is Federico Masiero from Sant 'Anna University, in Pisa, Italy [18].

To calculate the magnetic flux that passes through the coil, it was necessary separate the different magnetic flux density field components. Only the perpendicular component to the coil was counted. The simulated magnetic field comprises two components: the B_{axial} and B_{radial}, as shown in Figure 35.

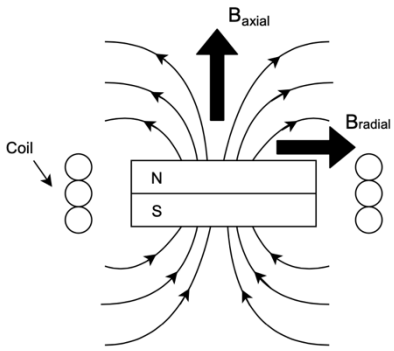

Figure 35- Magnetic flux density field components.

The simulation to find the best coil location had to be based on the component perpendicular to it (B_{axial}), presented next in Figure 36.

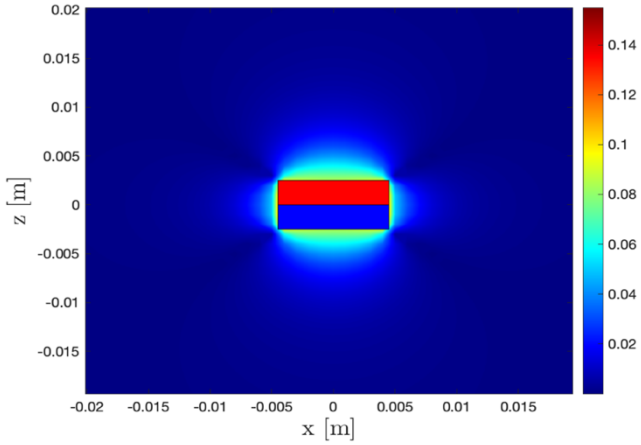

Figure 36- B_{axial} magnetic flux density component (Tesla).

With the correct simulation, the device can be optimized and two characteristics can be changed to guarantee the device's maximum efficiency; the diameter of the coil (D) and the distance to the magnet (DM), which is the distance the centre of the coil and the centre of the magnet. They are presented in Figure 37.

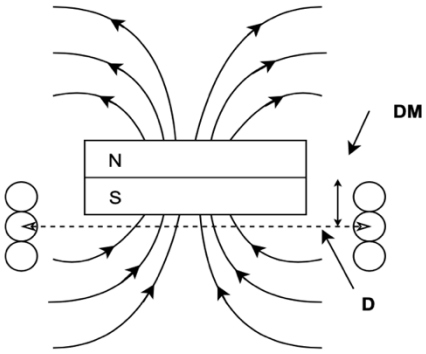

Figure 37- Schematic of the characteristics to be optimize.

The first step in finding the ideal dimensions of the coil diameter and distance to the magnet was to vary them in a three-dimensional graph and observe the magnetic flux values (Figure 38).

The coil diameter varied between the minimum value, 12mm, to 45mm; and the distance to magnet from the point where the centre of the coil is aligned with the magnet's centre (0mm) to 45mm.

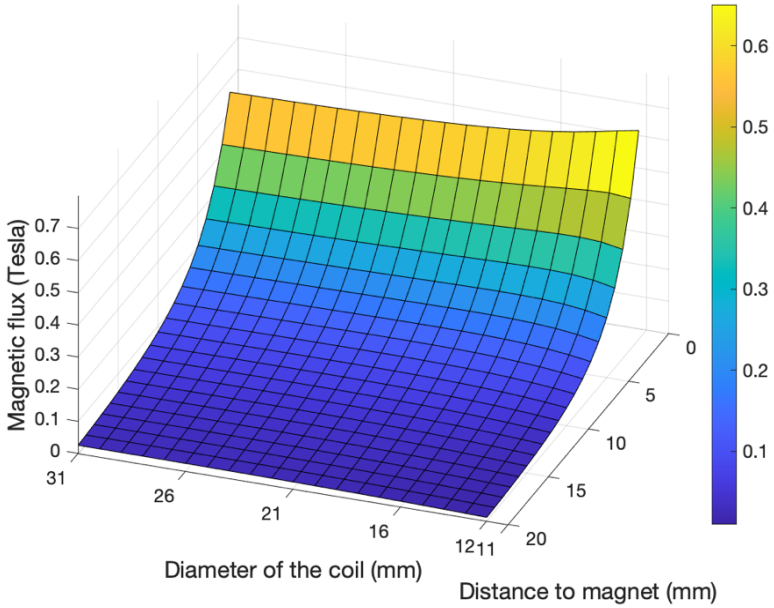

Figure 38- Magnetic flux density in order to diameter of the coil and the distance to magnet.

From the graph above, it is possible to conclude that the maximum magnetic flux value is when the distance to magnet is 0 mm, and when the diameter is 12mm, being an acceptable result up to 15 mm.

The same process was then carried out, but now, deriving the magnetic flux to see where the magnetic flux had a more significant variation, because the variation in magnetic flux will be proportional to the voltage induced in the coil. The derivate of the magnetic flux can be seen in the next Figure 39.

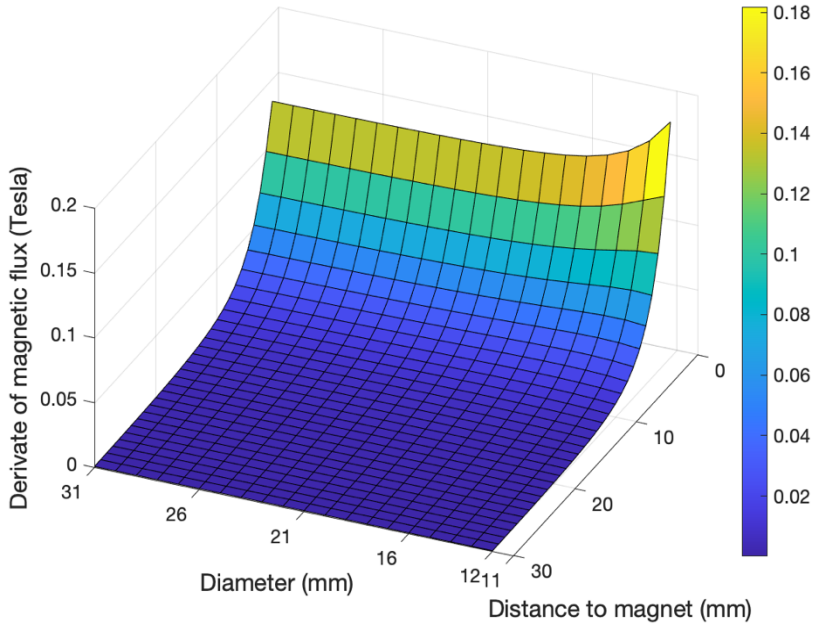

Figure 39- Magnetic flux density variation in order to diameter of the coil and the distance to magnet.

From the results presented it is possible to conclude that the distance to magnet where the flux variation is maximum is also 0 mm. However, it is now more pronounced than the coil's ideal diameter is 12 mm.

After analysing the behaviour of the magnet and the place where it is best to set the coil concerning the magnet, the transducer began to be elaborated, which was one of the objectives of this thesis.

The elaborated transducer followed the basis of the Magnetic Levitation Vibration Energy Harvesting type but with some modifications. The top magnets are fixed in the Magnetic Levitation Vibration Energy Harvesting transducer, which means the distance between the two top magnets is always the same. In the elaborated transducer, the distance between magnets can be adjusted to optimize the transducer and obtain more energy with the same vibration source. The dimensioning of the internal cylinder of the transducer was not exactly the same diameter as the magnet, it was a little wider due to difficult mechanical conditions in its production. Then, the transducer could not be designed to hold only one levitation magnet, because the inner cylinder was a little wide, and the magnet in the centre turned, due to the attraction and repulsion force from the top magnets. It was then necessary to increase the number of magnets in the levitation, which could be done with two or three central magnets. So, the transducer elaborated consists of a coil with 200 windings, five or four magnets with 15mm in diameter, and 3mm in height with 860-995 kA/m of magnetization that they were inside a polycarbonate cylinder, two 3D printed parts, and two screws, as explained in the sub section 3.2.

These parts were attached to the transducer cylinder with hot glue, which allowed them to be easily removed to test the transducer with two or three central magnets.

Each of the two top magnets was connected to a screw, with hot glue, that can modify its position. This capability can manipulate the central magnet's position regarding the coil due to the phenomenon of levitation and the distance of the top magnets between them. This adjustment was possible because the printed tops were designed for this purpose. The final result after assembly is shown in Figure 40.

Figure 40- Transducer all assembled.

Chapter 5 Results

This chapter will present the transducers analysis results based on both programs elaborated, one to characterize the transducer and the other to test the transducer in emulated sources.

5.1 Transducer Characterization Results

The first results come from the first version of the program, where a sine wave of 2V peak-to-peak amplitude was selected with the frequency varying between 1 and 100 Hz, linearly with a step of 1 Hz. Figure 41 shows the value of the vibration acceleration caused by the selected wave and applied to the stimulation chain.

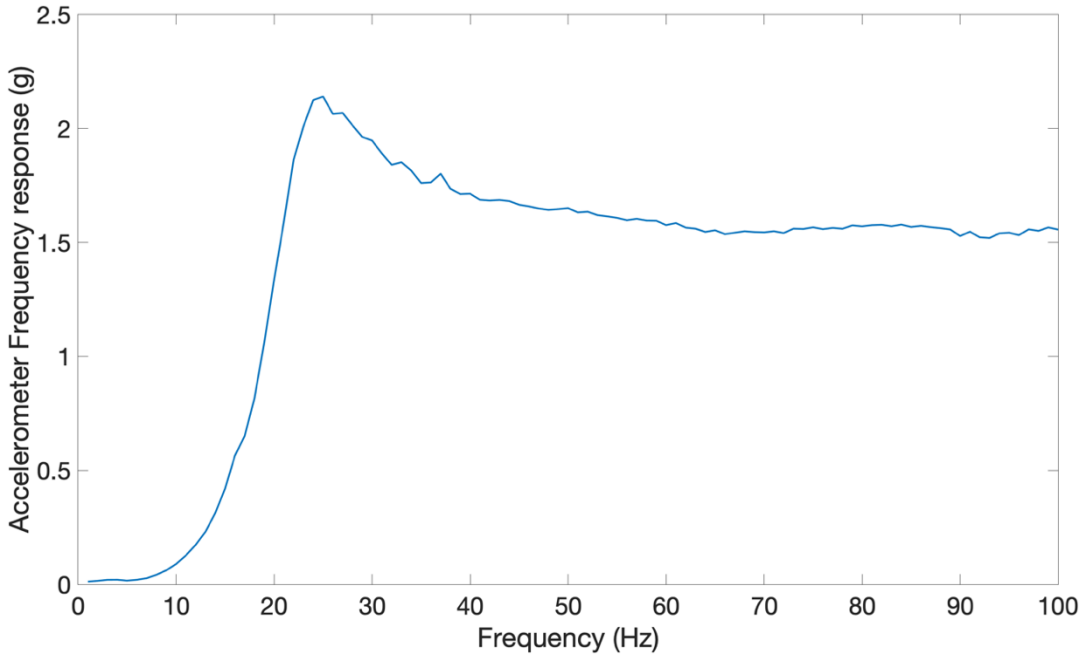

Figure 41- Accelerometer response by the selected signal.

Then, the amount of power that the transducers can generate was analysed by varying the distance between the top magnets, making a frequency and load resistance sweep. The frequency sweep was linear between 10 and 100 Hz with a 1 Hz step, and the load resistance sweep was logarithmic that vary between 1 ohm and 10K ohm in 20 points.

The analysis started by testing the generated power when the transducer had three central magnets centred with the coil and varying the distance between the top magnets. Starting with the top magnets at a distance of 6 cm, which was as far apart as possible due to the transducer characteristics, and ending at 4 cm, which was as close as possible also due to the transducer characteristics. Figures 42 to 46 show the result of this test where the distance between top magnets was varied from 6 cm to 4 cm with a step of 0.5 cm.

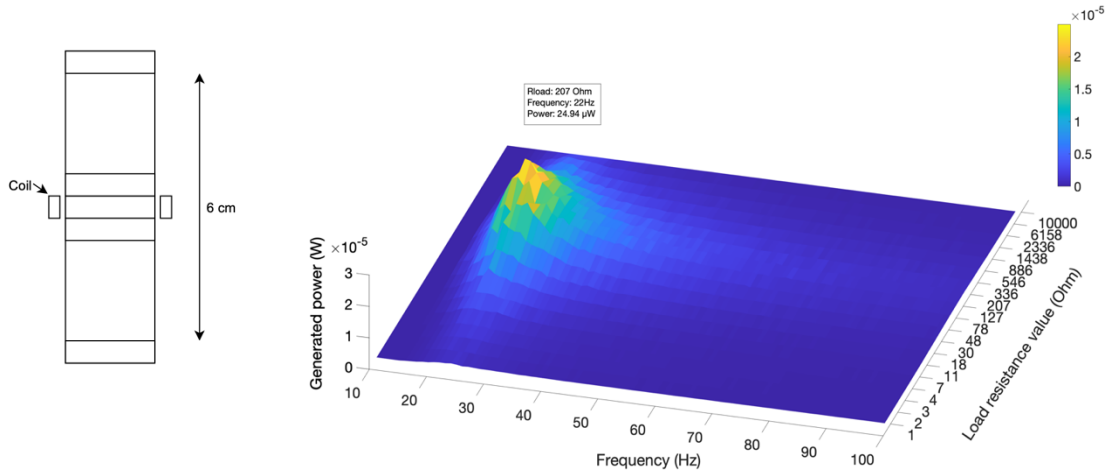

Figure 42- Power generated with 6 cm between top magnets. magnets.

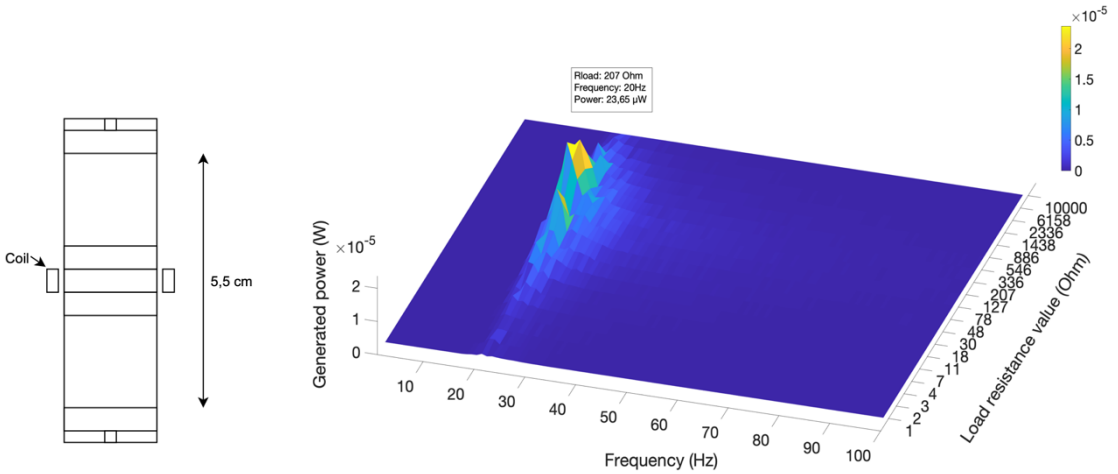

Figure 43- Power generated with 5,5 cm between top magnets.

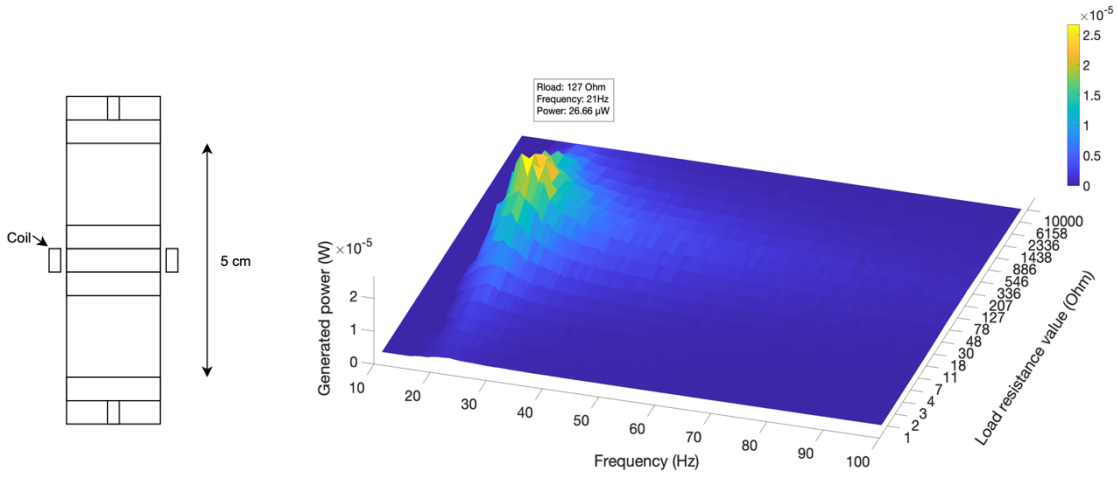

Figure 44- Power generated with 5 cm between top magnets.

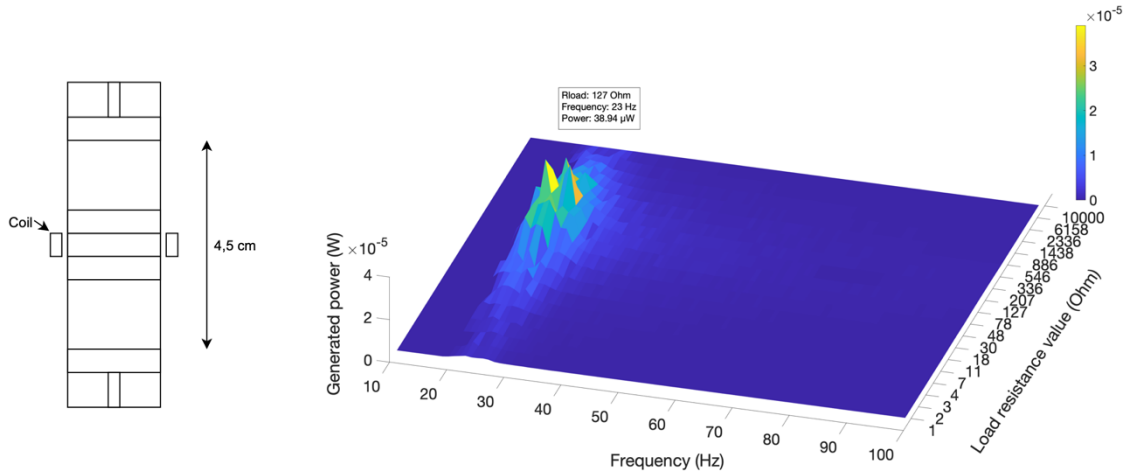

Figure 45- Power generated with 4,5 cm between top magnets.

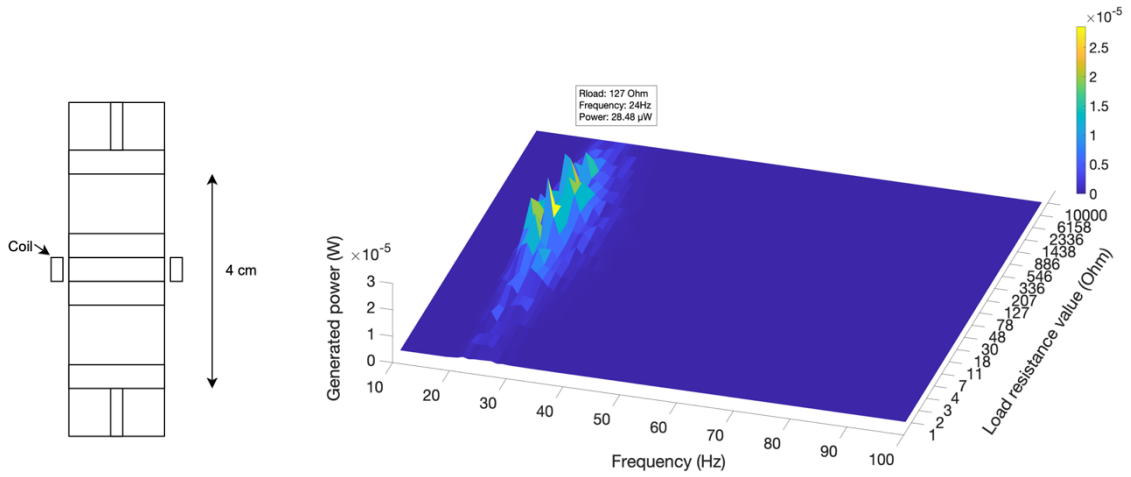

Figure 46- Power generated with 4 cm between top magnets.

From this test can be concluded that it is possible to generate power values between 23.65 µW and 38.94 µW for the wave imposed in the stimulation chain. The maximum power in each distance variation between the top magnets is always reached in the frequency range between 20 Hz and 24 Hz and load resistances between 127 ohm and 207 ohm. The distance between magnets provides the best power result is 4.5cm It was important to find this optimization point because if the repulsion force between each top magnet and the central ones were too small, the central magnets when moving would deviate from the coil, which did not brought good results and if the repulsion force between each top magnet and the centre magnets was too great, the centre magnets remained static, thus not generating magnetic induction.

After understanding the ideal distance between top magnets to optimize the power value, the next test was to know the influence on the generated power if the magnets were no longer centered with the coil. So, keeping the ideal distance between magnets, the position of the magnets relative to the coil was varied. Each variation and respective power generated can be observed in Figures 47 to 50.

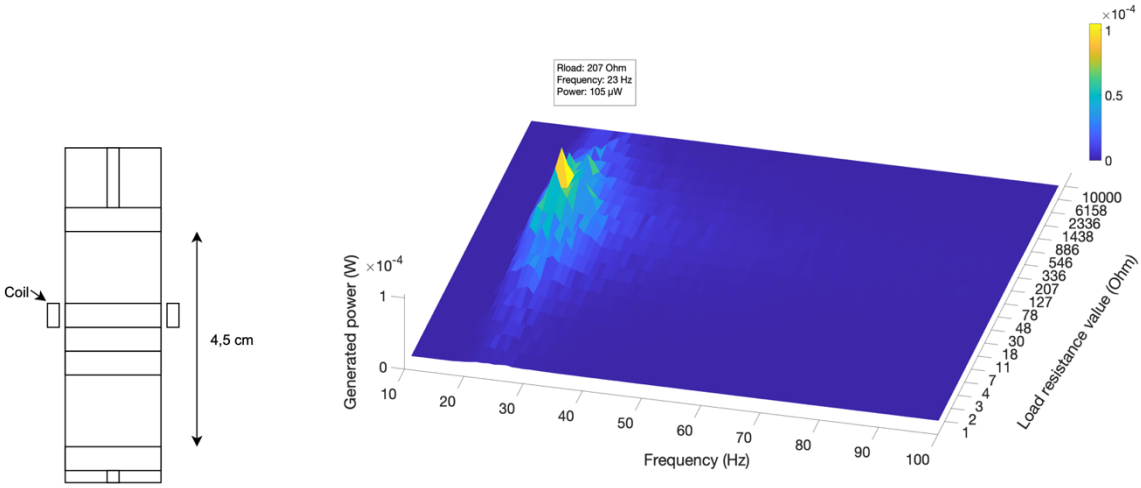

Figure 47- Power generated when the central magnets rise by 3 mm.

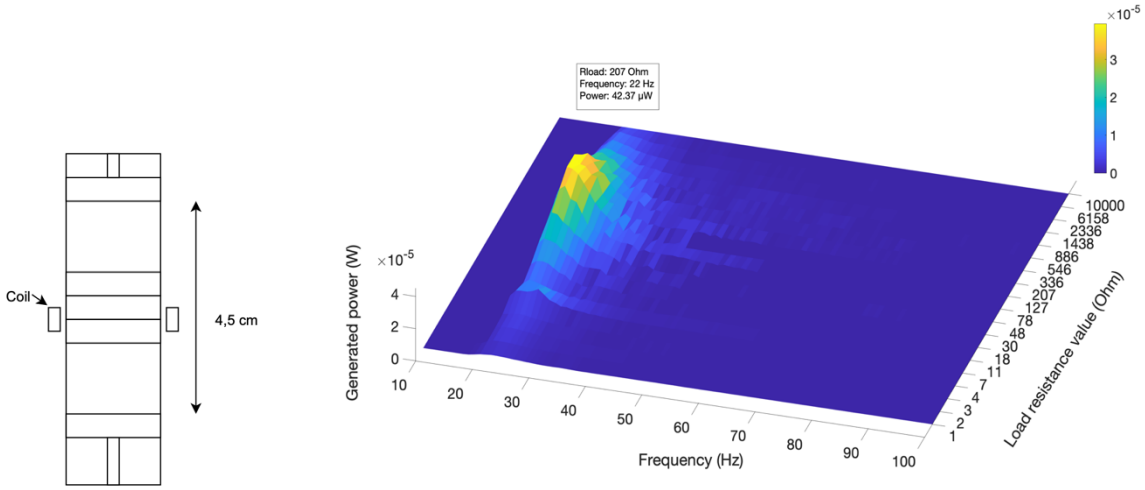

Figure 48- Power generated when the central magnets drop by 1.5 mm.

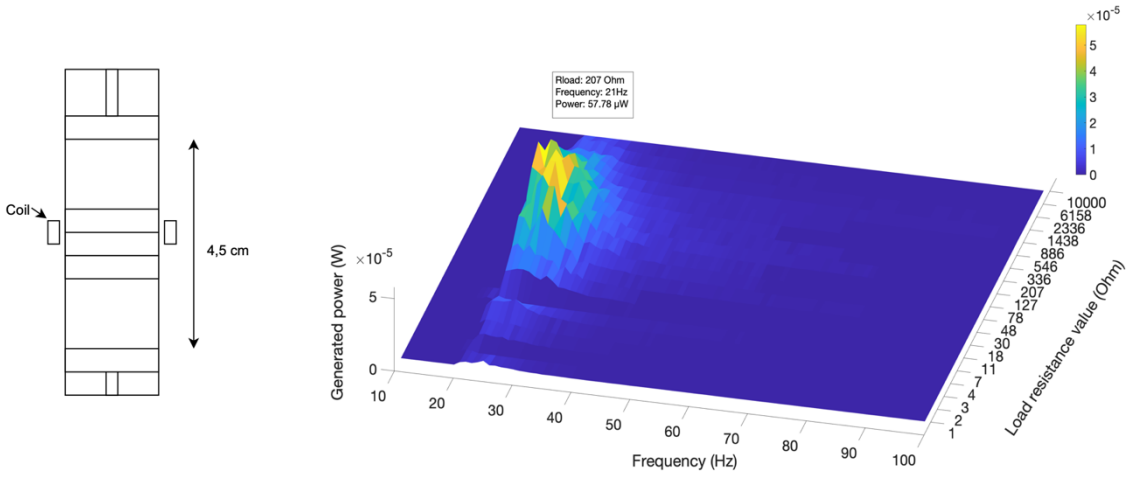

Figure 49- Power generated when the central magnets rise by 1.5 mm.

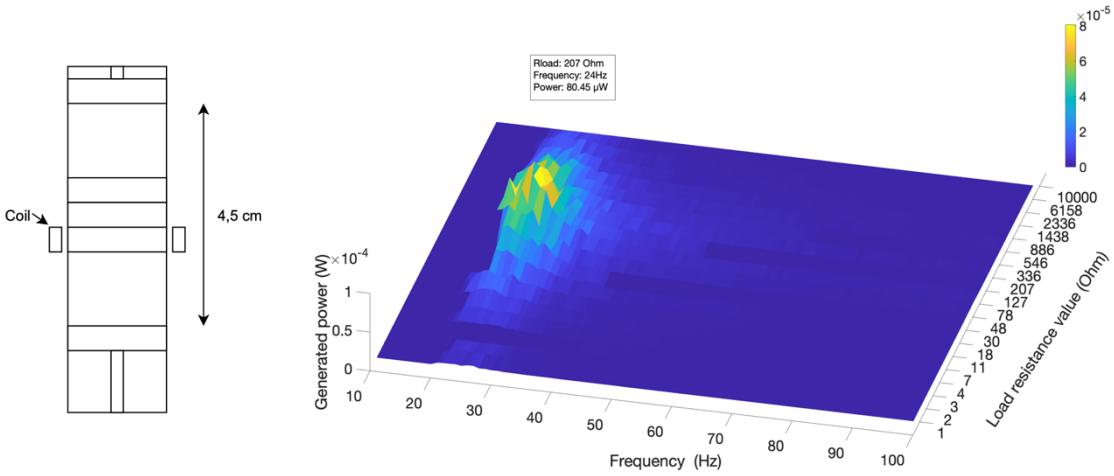

Figure 50- Power generated when the central magnets drop by 3 mm.

This test concluded that the power generated was lower when the magnets were centered with the coil. This happens because the three central magnets worked as a single magnet with 9mm of height, and in the area where the coil was located, the magnet's magnetic field had no perpendicular component gradient. The generated power became greater as the extremities of the moving magnets approach the coil, reaching its maximum when the coil was aligned with the upper magnet. This was where the perpendicular component to the coil was strongest, such as when the lower magnet was aligned to the coil.

However, when the lower magnet was aligned to the coil, due to gravity, when the magnet oscillates, it went out of reach of the coil, thus lowering the generated power to 80.45 μW, a little less than 105 μW than was the maximum power generated. When the coil was placed between the center and the top magnet and between the center and the bottom magnet values of 57.78 μW and 42.37 μW, respectively, were obtained. To understand the influence of the vibration acceleration on the electromotive force created, Figure 51 shows the transducer transfer function for the best case, when it generates a power of 105 μW.

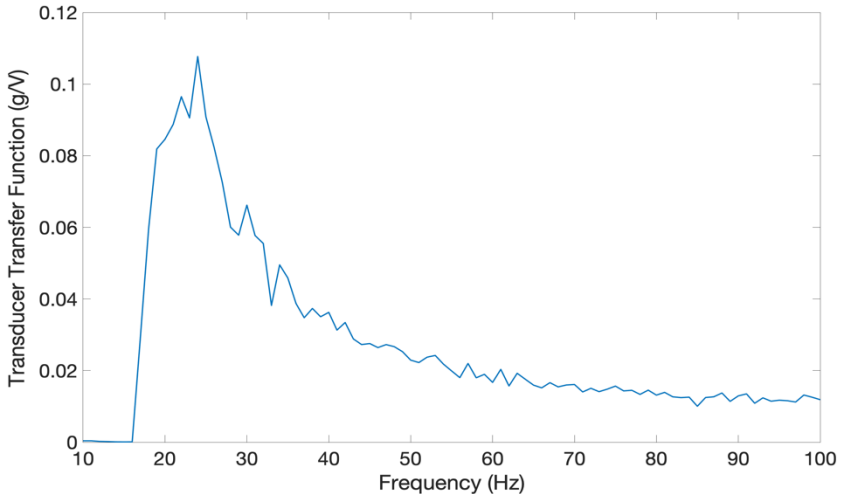

Figure 51- Transducer transfer function.

After knowing the behaviour of the transducer with three central magnets. The transducer was tested still with the first program version with two central magnets with precisely the same stimulus as the previous tests, a sinusoidal wave of 2V peak-to-peak amplitude with the frequency varying between 1 and 100 Hz, linearly with the 1 Hz step. First, the distance between the top magnets centred with the coil was varied, also between 6cm and 4cm, with variations of 5mm in 5mm, and the result is visible in Figure 52 to Figure 56.

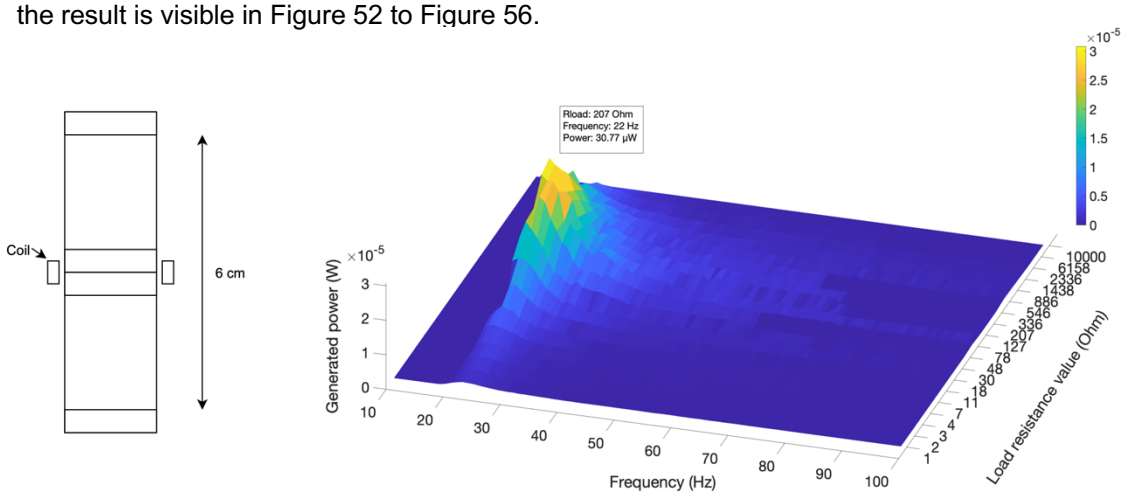

Figure 52- Power generated with 6 cm between top magnets.

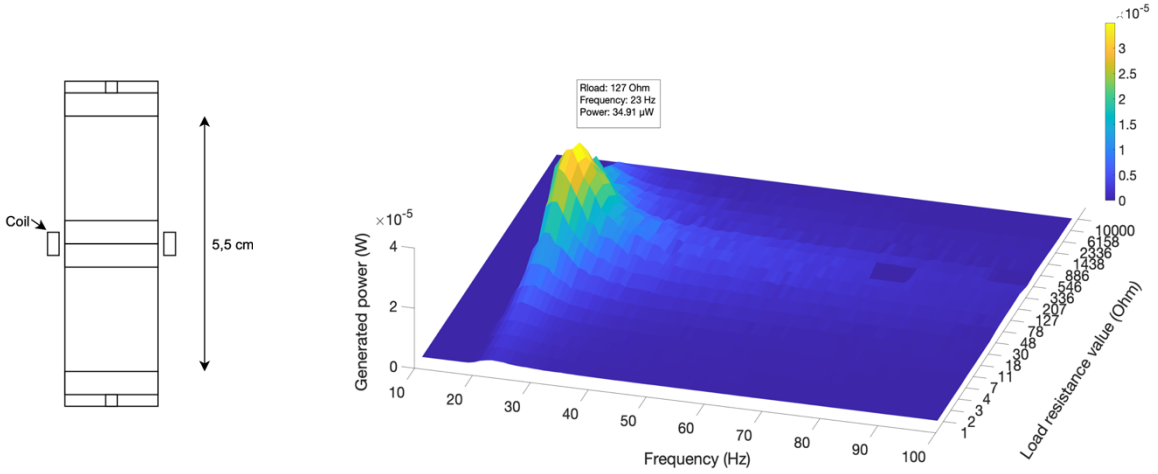

Figure 53- Power generated with 5,5 cm between top magnets.

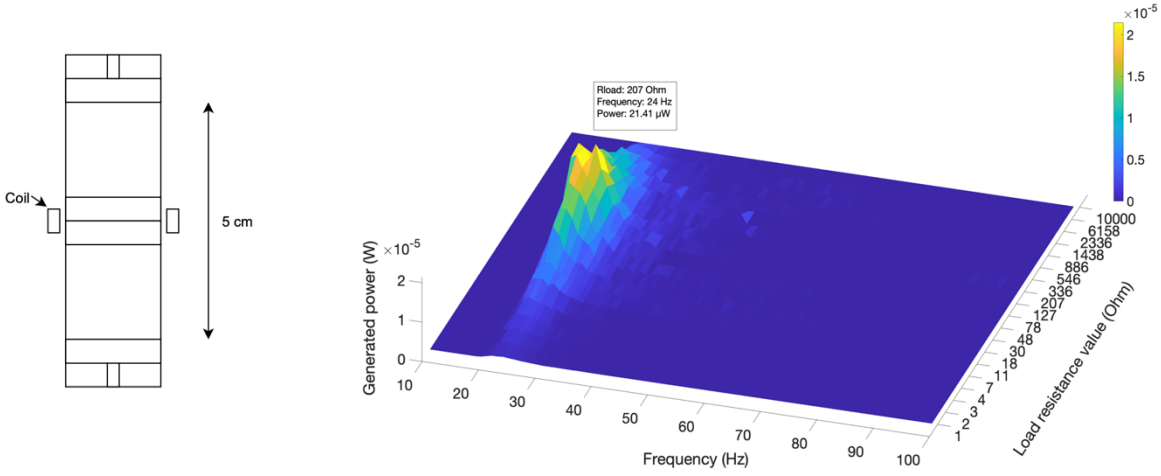

Figure 54-Power generated with 5 cm between top magnets.

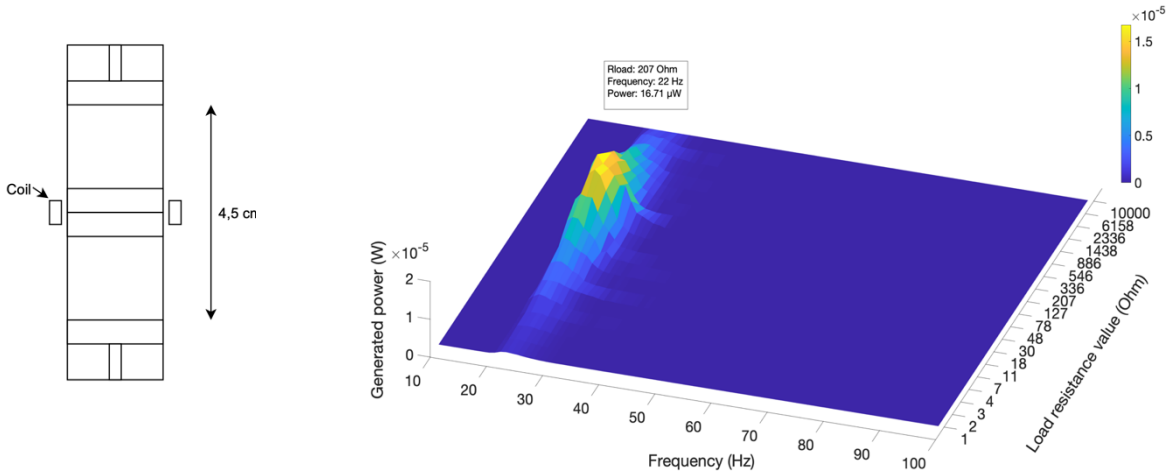

Figure 55-Power generated with 4,5 cm between top magnets.

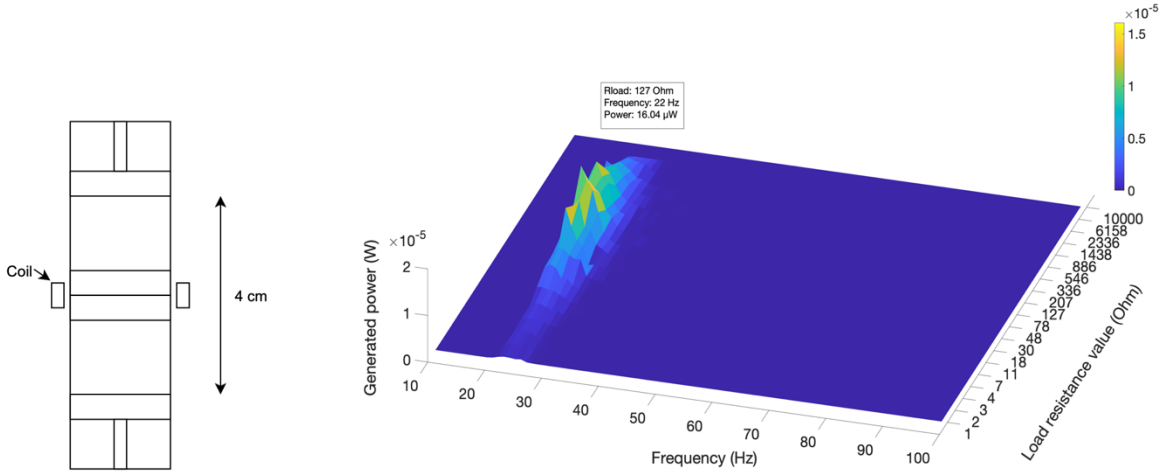

Figure 56- Power generated with 4 cm between top magnets.

With two center magnets aligned with the coil, the maximum generated power was 34.91 uW when the top magnets were at a distance of 5.5 cm at a frequency of 23 Hz and with a load resistance of 127 ohm. The optimal frequencies ranged between 22 Hz and 24 Hz and load resistances between 127 ohm and 207 ohm for the other distances. The optimal distance was 5.5cm with two central magnets, while with three central magnets, it was 4.5cm. This is explained by the smaller weight with two magnets, so the repulsion force needed to stabilize the central magnets was minor. This stabilization was necessary for the optimization of the results, as explained above. Once find the optimal distance between the top magnets, the position of the center magnets concerning the coil was varied to find out if the results followed the trend of the transducer with three center magnets or a different register. In this case, it only made sense to test two positions, with the coil centered with the bottom magnet and with the top magnet, shown in Figures 57 and 58, respectively.

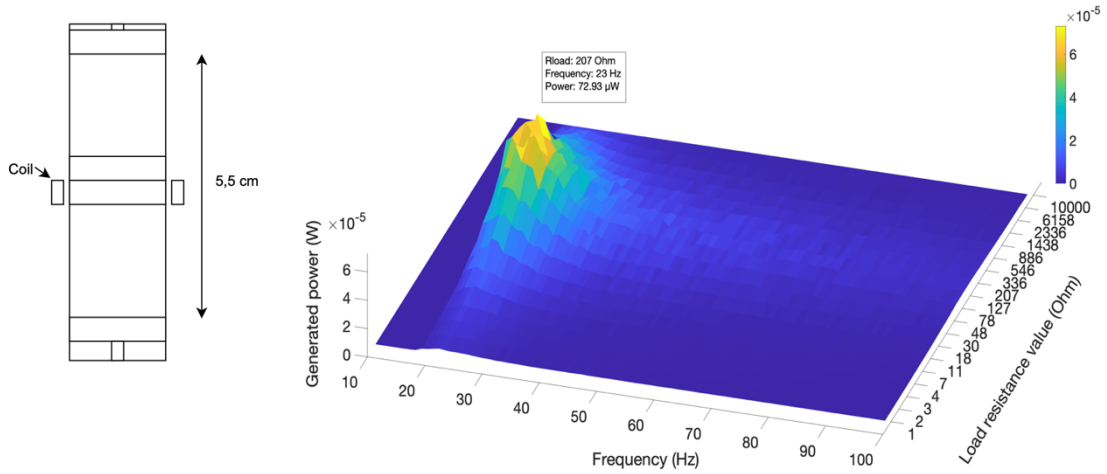

Figure 57- Power generated when the central magnets drop by 1,5 mm.

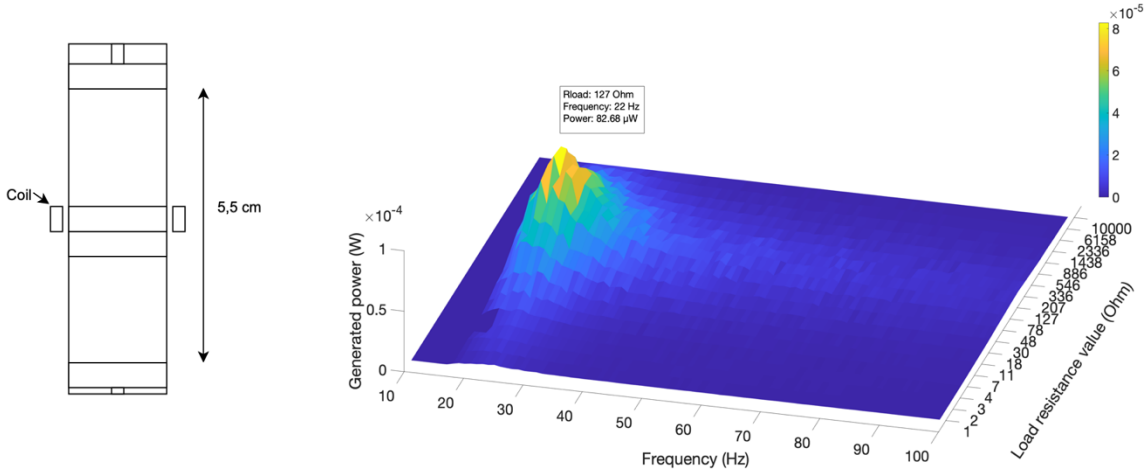

Figure 58-Power generated when the central magnets rise by 1,5 mm.

After analyzing the transducer with three and two centre magnets, the results are presented in Figure 59 where it can be observed the generated power by each distance between top magnets in both cases.

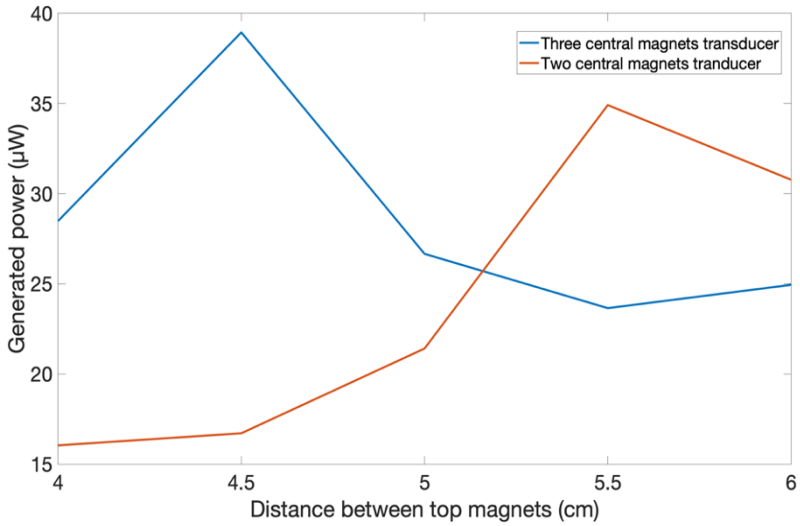

Figure 59- Maximum power generated at each distance.

It is concluded by observing the graph that there is an optimal point where the transducer can generate more energy in each case. In the case that it had three central magnets, the optimal distance was 4.5 cm between the top magnets, and in the case that the transducer had two central magnets, the ideal distance was 5.5 cm between the magnets of the tops. This difference happened because the weight of the central magnets was obviously different, which requires different intensities of the repulsion force that allows the levitation at each case.

When the transducer had three central magnets, the negative influence of the distance between the top magnets was very evident. This happened because the repulsion force between the top magnets and the central magnets was very small, originating very large oscillations by the central magnets regarding the coil, thus leaving the range of the coil and generating less energy.

On the other hand, it was very evident in the transducer when it had two central magnets the negative influence of the excessive approximation between the top magnets and the center magnets. It happens because the repulsive force between the top magnets and the center magnets was so great that it did not allow the central magnets to respond to the vibration stimulation by moving because they were stuck by the repulsive force acting on it thanks to the proximity of the top magnets.

Regarding the energy that the transducer could generate with two or three central magnets at the distances between top magnets tested, when the central magnets were centered with the coil the transducers had identical results at ideal distances.

Next, the results of the central magnets position variation relative to the coil in the transducer with two and three central magnets were compared. When the transducer had three central magnets, the displacements tested were when the central magnets go down and up 1.5 mm and 3 mm regarding to the center, and when the transducer had two central magnets, the displacements tested were only when the central magnets go down and up 1.5 mm regarding to the center. The maximum power generated at each displacement for both cases can be observed in Figure 60.

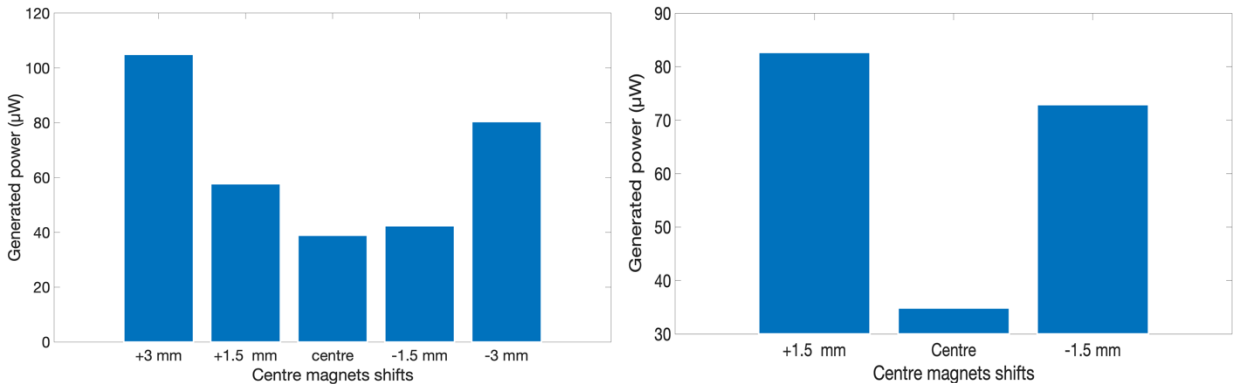

a) Three centre magnets displacement. b) Two centre magnets displacement.

Figure 60- Maximum generated power at each displacement.

As the Figure shows, the lowest power values were recorded when the central magnets were aligned with the coil, and the highest values when the center of the central magnets was moved so that the extremities magnets, the top or bottom, line up with the coil. This phenomenon happens because when

the magnets were together, due to the attractive force between equal poles, this set worked as just one magnet. Therefore, it only presented a significant magnetic field perpendicular component gradient to the coil at the extremities.

The coil had 3 mm of height, exactly the same as each centre magnet height, which indicates that when the centre magnets moved 3mm down or up on the three centre magnets transducer, the coil became aligned with one of the extremities magnet, which was precisely where the component perpendicular to the coil of the magnetic field was strongest. This fact explains that, it is in these position that the transducer achieves the highest power results. The transducer with two center magnets had the same behaviour, it also had the highest power values when aligning the end magnets with the coil.

It was also easier to stabilize the three central magnets in the ideal position because it brought better results. While with two central magnets, the collected power was a bit lower, indicating a less successful stabilization.

The knowledge of the transducer behaviour was essential as it allows to conclude the distance between top magnets and in which position relative to the coil the central magnets should be to obtain an optimized power result. After this learning, the two central magnets transducer will be tested in real sources emulated by the vibration generator.

5.2 Evaluation of Emulated Vibration Sources Results

These results were achieved through the second part version of the program, responsible for testing the transducer on real vibration sources simulating them in the vibration generator. The vibration sources chosen to emulate in the vibration generator were the movement during walking of the lower leg, the water pump motor, and the car's engine.

As mentioned in the 3.5.2 section, the characteristic data of each vibration to be simulated was taken from an online repository, so the data measured through the accelerometer installed in the coupling mechanism would have to be as similar as possible to the one taken from the repository. The process carried out in the "wave program" tab in the LabVIEW program brought results slightly different from the target. So it was necessary to approximate the target wave and the measured wave as much as possible. To do this, the optimization tab in the LabVIEW program was run. After it was no longer possible to approximate the result, the EMF by each frequency and the power by each load resistance were then calculated.

The first source to simulate was the lower leg movement when walking, whose results can be seen in Figures 61 and 62. Figure 61 shows the optimization process at each iteration and the final signal measured by the accelerometer. Figure 62 shows the differences between the measured signal and the target signal spectrum and the electromotive force that the transducer can generate from the simulated source.

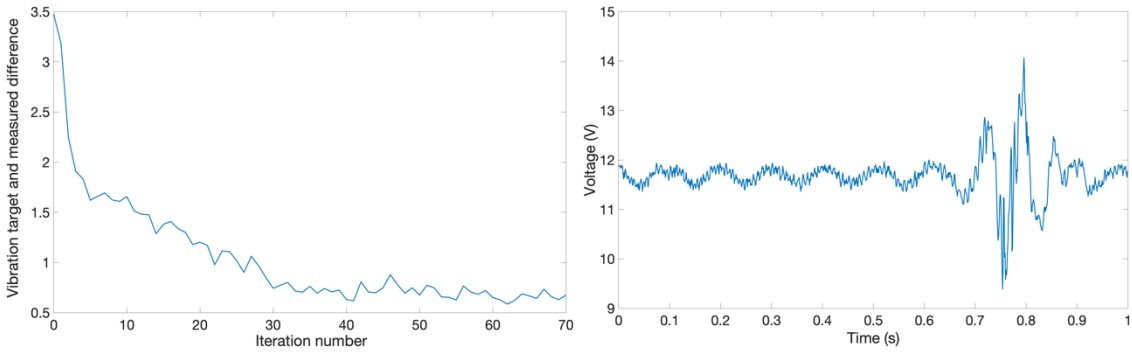

Figure 61- Optimization process and resulting signal.

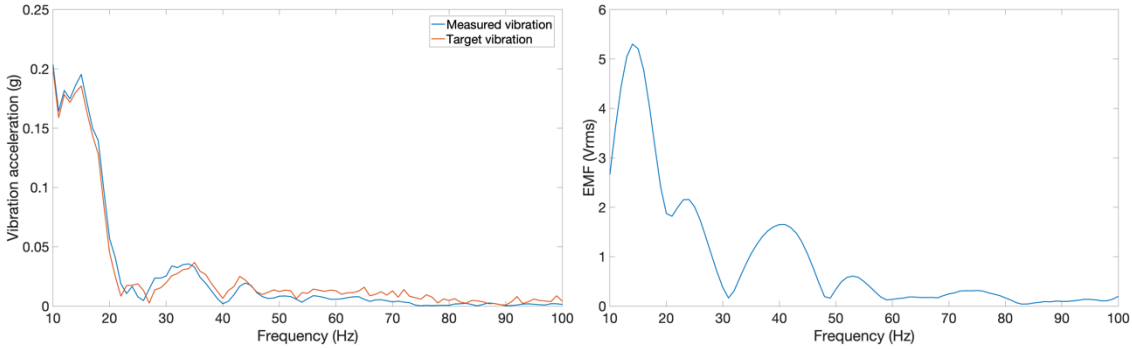

Figure 62- Measured and target vibration and EFM resulted.

As shown in Figure 61, the optimisation process was demanding. It took about 40 iterations to present a reliable result of the simulated source, reaching the final signal, also visible in Figure 61. In Figure 62, a comparison between the target signal and the signal that the accelerometer measures after the optimisation process is visible. The optimisation process achieved a good approximation, so the transducer tested on the chosen source managed to generate a maximum EMF of 5,2 $V_{rms,}$ also visible in Figure 62.

Another source simulated in the vibration generator was the car engine, whose results of this simulation can be evaluated in Figures 63 and 64. In Figure 63, the optimization process at each iteration and the final signal measured by the accelerometer that measures the vibration generator vibration. And in Figure 64, the overlapped graphs of target and measured vibration together with the electromotive force generated in this simulated source.

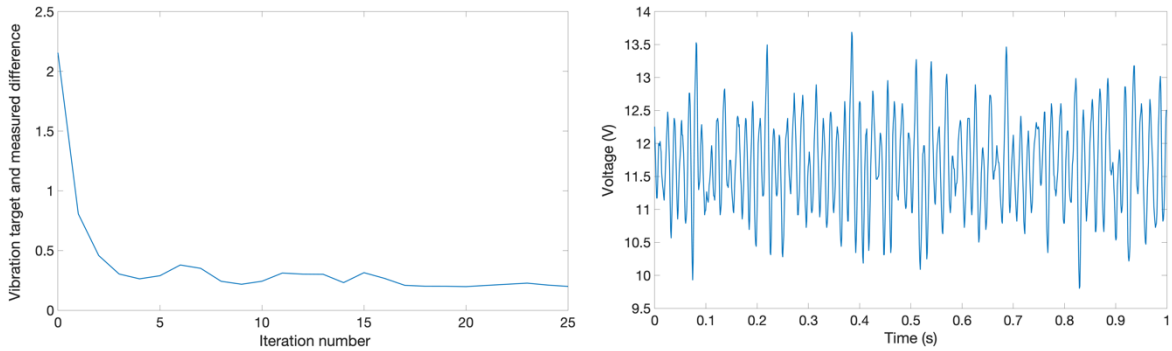

Figure 63- Optimization process and resulting signal.

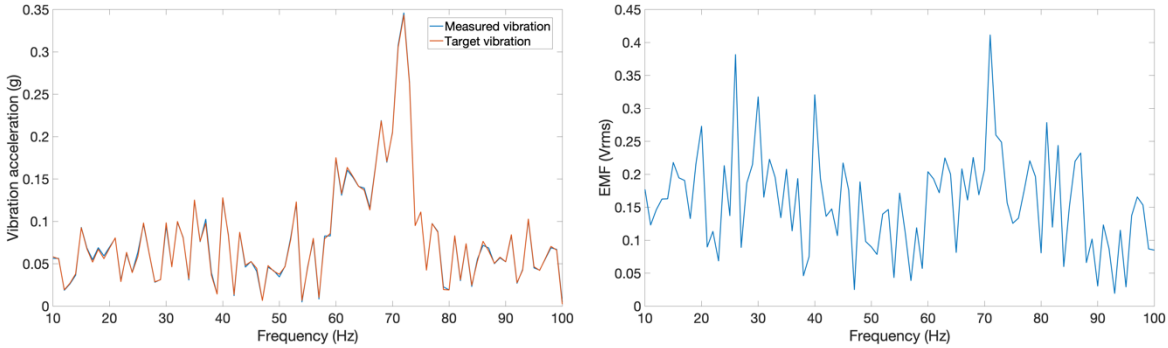

Figure 64- Measured and target vibration and EFM resulted.

The optimization process of this source was easier than the previous one, as it is visible in Figure 63, in the fourth iteration, the obtained signal was already very close to the final signal. This signal is also visible in Figure 63. In Figure 64, it is visible that the process of optimization was successful because the differences between the target and acquired signal are minimal, thus making a good replication of the vibration source to be simulated. Also, in Figure 64, it is possible to consult the EMF that the transducer could generate applied to this simulated source. It was possible to reach maximum EMF values in the order of 0,042 V_{rms}, values higher than those reached with the previous simulated source.

The last tested source was the water pump motor, which results are shown in the same way as the sources presented above. Results are present in Figures 65 and 66. Figure 65 shows the optimization process at each iteration and the final signal acquired by the accelerometer that measures the vibration of the vibration generator. Figure 66 shows the overlapped graphs of target and measured vibration to compare them and see if the optimization process was successful and the electromotive force that the transducer can generate applied to this source.

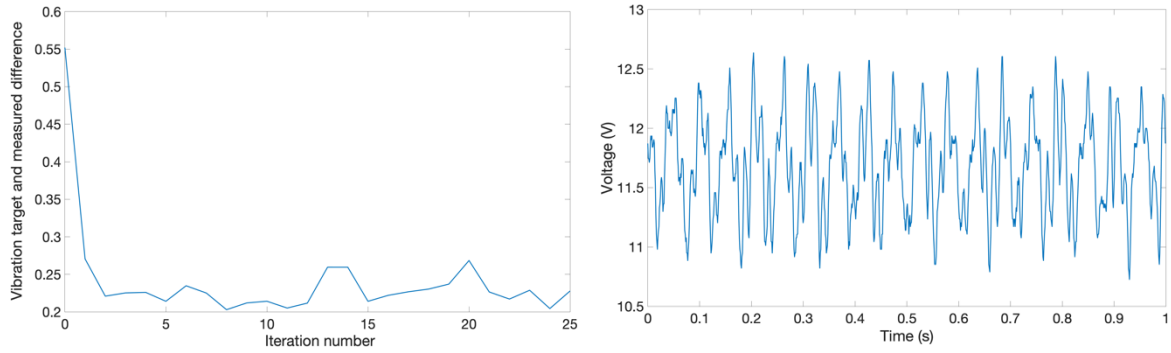

Figure 65- Optimization process and resulting signal.

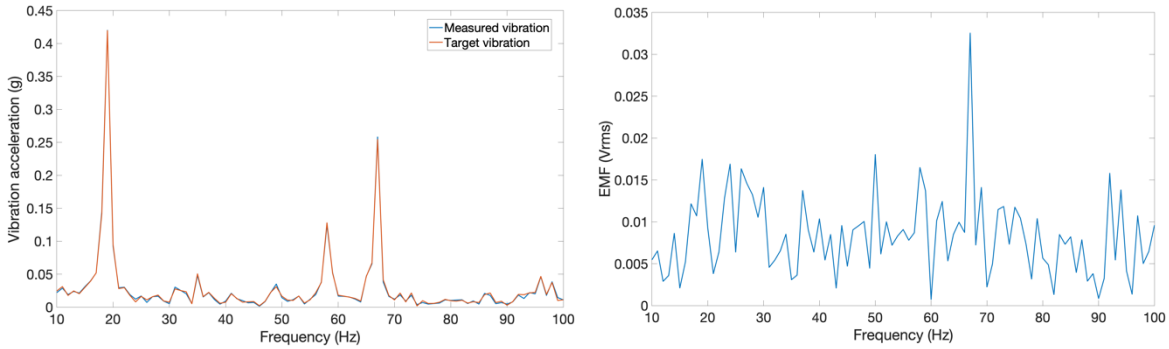

Figure 66- Measured and target vibration and EFM resulted.

The optimization process visible in Figure 65, similarly to the previous source, quickly converged to the result obtained at the end of the optimization that originated the signal, also visible in Figure 65. The objective of simulating the source in the vibration generator was successful because as shown in Figure 66, the vibration signal done by the vibration generator was very similar to the target signal. It is also visible in Figure 66 the EMF that the transducer was capable of generate when applied to the simulated vibration source. The EMF that the transducer can generate happens with a frequency of 68 Hz, and it is about 0.034 V_{rms}.

The results presented show that the objective of this part of the program was successfully completed, since it was possible to simulate the desired sources accurately and also to test the transducer on them. The key factor that led this test to success was the optimization tab, since only the result of the “wave programming” tab did not respond to the initial challenge of an authentic simulation.

After presenting the simulation characteristics of each of the analysed sources, it was also determined the power that each source would be able to generate, varying the load resistance at the transducer terminals. A linear sweep of the load resistance value was performed in all cases to analyse the influence of that at the transducer terminals. The results of this test can be seen in Figure 67.

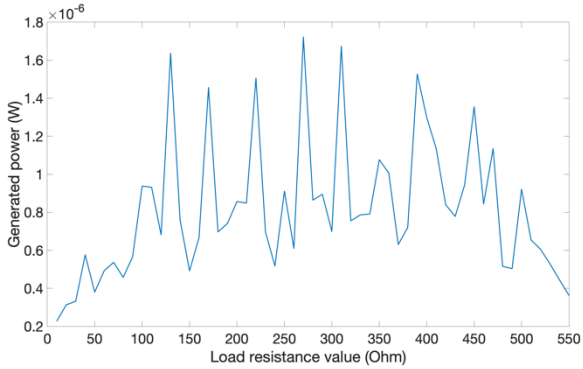

a) Lower leg.

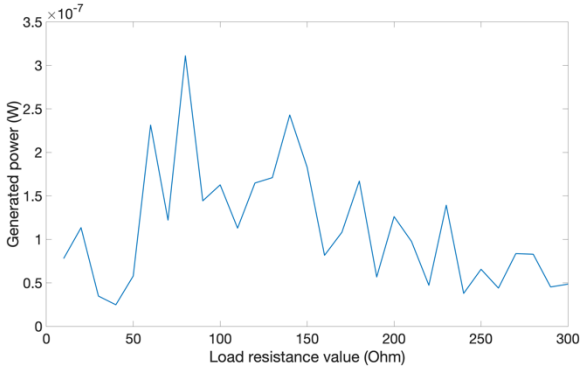

b) Water pump motor.

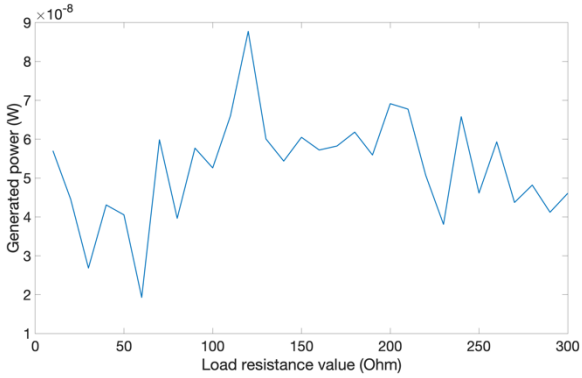

c) Car engine.

Figure 67- Power generated by each vibration source.

The results of power that the transducer can generate in each source of vibration vary for the source of lower leg walking between 0,4 uW and 1,7 uW, reaching its maximum with a load resistance of 275 ohm. When applied to the water pump motor, the transducer can generate between 0,025 uW and 0,33 uW, reaching its maximum power output with a load resistance at the transducer terminals of 80 ohm. When the car engine was simulated reached about 0,0088 uW at its maximum and a lowest value of 0,002 uW.

Chapter 6 Conclusion

6.1 Summary and Achievements

Energy can be harvested from a wide variety of sources and an alternative of the use of batteries to power the devices, it is the use of energy sources presented in environment like solar energy, thermal energy, wind energy, vibration energy, amongst others. Currently, it is increasingly necessary to recover all the energy possible, both ecologically and economically. Vibration is an example of an energy source that is rarely used, but with a great potential in the production of energy.

Vibration energy can be harvested mostly through piezoelectric, electrostatic, and electromagnetic transducers. Electromagnetic transducers harvest the vibration energy based on electromagnetic induction phenomenon. Levitation electromagnetic transducer type energy harvester was the chosen transducer topology to build and characterize because it avoids using the springs to make the magnets move, which brings the buckling effect to the transducer. Furthermore, it can be implemented in several situations and locals, and it does not require any specific vibration or movement.

To be possible to analyse and characterize the transducer, it was necessary to build a setup characterization capable to do it. This characterization setup consisted of two parts, the hardware part and the software part. The hardware part was composed by the necessary instrumentation to control and process the transducer behaviour, and the software part was programmed in the LabVIEW software and its goal was to control the devices present in the hardware part and receive data from the system that would allow both the analysis and the characterization of the transducer ability to generate energy. Two separate programs were made in LabVIEW. One with the objective of optimising the results of the transducer, analysing at what distance the top magnets should be located and the position of the central magnets relative to the coil to achieve the maximum energy possible generated by the transducer. On the other hand, the second one with the objective of simulating several sources in the vibration generator, based on vibration data from real sources obtained data banks, and thus test the transducer on these real sources without leaving the laboratory. With these experiments, we can conclude that the initial aim of developing instrumentation to characterize the transducers and to emulate operational conditions when included on a IoT device was concluded with success.

The objective of illustrating the design and prototyping of an induction-based vibration energy transducer was also achieved however the transducer characteristics can be improved in the future.

6.2 Future work

This sub-section addresses some of the improvements whose aim is to repair the limitations of the system and improve the system's overall functioning:

- To replace the DAQ used by one with greater capacity and acquisition rate, in order to improve the performance and speed of the code.
- The function generator used had limitations at the arbitrary wave programming level, which only receives 1024 points for each arbitrary wave programmed, with a resolution of only 10 bits. If this function generator can be replaced by one with a greater capacity in these areas, it would be possible to have a wave in its output more similar to the original wave.
- In the excitation chain, it is important to replace the amplifier used with one that did not limit the range of frequencies and a vibration generator capable of responding to a stimulus with vibrations at frequencies above 100 Hz.
- When constructing the transducer, it is necessary to dimension the internal cylinder to exactly match the diameter of the magnet used to be able to use only one magnet as central magnet, which will bring better results. It is also possible to improve the coupling system to the vibration generator, as the one used becomes a little loose with usage. The way the top parts are connected to the transducer can also be improved and the top parts and the screw can be updated to allow testing more distances between top magnets.

References

[1] Z. Chen, L. Zhu, W. Li, and S. Fan, “Simultaneously and Synergistically Harvest Energy from the Sun and Outer Space,” *Joule*, vol. 3, no. 1, 2019, doi: 10.1016/j.joule.2018.10.009.

[2] V. A. Gusarov and Z. A. Godzhaev, “Development of Low-Power Gas Turbine Plants for Use at Industrial Facilities,” *J. Mach. Manuf. Reliab.*, vol. 47, no. 6, 2018, doi: 10.3103/S1052618818060055.

[3] M. Tang, Q. Guan, X. Wu, X. Zeng, Z. Zhang, and Y. Yuan, “A high-efficiency multidirectional wind energy harvester based on impact effect for self-powered wireless sensors in the grid,” *Smart Mater. Struct.*, vol. 28, no. 11, 2019, doi: 10.1088/1361-665X/ab45fe.

[4] R. Das *et al.*, “Enhanced room-temperature spin Seebeck effect in a YIG/C60/Pt layered heterostructure,” *AIP Adv.*, vol. 8, no. 5, 2018, doi: 10.1063/1.5007233.

[5] M. Gasulla, F. J. Robert, J. Jordana, E. Ripoll-Vercellone, J. Berenguer, and F. Reverter, “A High-Efficiency RF Harvester with Maximum Power Point Tracking,” *Proceedings*, vol. 2, no. 13, 2018, doi: 10.3390/proceedings2131049.

[6] Z. Chen, Y. Yang, Z. Lu, and Y. Luo, “Broadband characteristics of vibration energy harvesting using one-dimensional phononic piezoelectric cantilever beams,” *Phys. B Condens. Matter*, vol. 410, no. 1, 2013, doi: 10.1016/j.physb.2012.10.029.

[7] W. Tian, Z. Ling, W. Yu, and J. Shi, “A review of MEMS scale piezoelectric energy harvester,” *Applied Sciences (Switzerland)*, vol. 8, no. 4. 2018, doi: 10.3390/app8040645.

[8] A. Mouapi, G. Vanessa Kamani, N. Hakem, and N. Kandil, “Multiphysics Simulation of Piezoelectric Cantilever Beam: Application in Automobile,” *Mod. Environ. Sci. Eng.*, vol. 3, no. 01, 2017, doi: 10.15341/mese(2333-2581)/01.03.2017/005.

[9] S. W. Ibrahim and W. G. Ali, “A review on frequency tuning methods for piezoelectric energy harvesting systems,” *Journal of Renewable and Sustainable Energy*, vol. 4, no. 6. 2012, doi: 10.1063/1.4766892.

[10] S. Boisseau, G. Despesse, and B. Ahmed, “Electrostatic Conversion for Vibration Energy Harvesting,” in *Small-Scale Energy Harvesting*, 2012.

[11] Khan Academy, “What is Faraday’s Law?,” *Khan Academy*, 2020. .

[12] C. Wei and X. Jing, “A comprehensive review on vibration energy harvesting: Modelling and realization,” *Renewable and Sustainable Energy Reviews*, vol. 74. 2017, doi: 10.1016/j.rser.2017.01.073.

[13] M. C. Chiu, Y. C. Chang, L. J. Yeh, and C. H. Chung, “Numerical assessment of a one-mass spring-based electromagnetic energy harvester on a vibrating object,” *Arch. Acoust.*, vol. 41, no. 1, 2016, doi: 10.1515/aoa-2016-0012.

[14] M. A. Halim, H. Cho, M. Salauddin, and J. Y. Park, “A miniaturized electromagnetic vibration energy harvester using flux-guided magnet stacks for human-body-induced motion,” *Sensors Actuators, A Phys.*, vol. 249, 2016, doi: 10.1016/j.sna.2016.08.008.

[15] K. Kecik, A. Mitura, S. Lenci, and J. Warminski, “Energy harvesting from a magnetic levitation system,” *Int. J. Non. Linear. Mech.*, vol. 94, 2017, doi: 10.1016/j.ijnonlinmec.2017.03.021.

[16] K. Kęcik, “Energy recovery from a non-linear electromagnetic system,” *Acta Mech. Autom.*, vol.

12, no. 1, 2018, doi: 10.2478/ama-2018-0002.

[17] University of Southampton, "Next Generation Energy-Harvesting Electronics: Holistic Approach" [online]. Available: http://www.holistic.ecs.soton.ac.uk

[18] S. Milici, M. Gherardini, F. Clemente, F. Masiero, P. Sassu, and C. Cipriani, “The myokinetic control interface: How many magnets can be implanted in an amputated forearm? Evidence from a simulated environment,” *IEEE Trans. Neural Syst. Rehabil. Eng.*, vol. 28, no. 11, 2020, doi: 10.1109/TNSRE.2020.3024960.